Three-dimensional ocular kinematics underlying binocular single vision

Hess, B J M ; Misslisch, H

Abstract: We have analyzed the binocular coordination of the eyes during far-to-near re-fixation saccades based on the evaluation of distance ratios and angular directions of the projected target images relative to the eyes' rotation centers. By defining the geometric point of binocular single vision, called Helmholtz point, we found that disparities during fixations of targets at near distances were limited in the subject's three-dimensional visual field to the vertical and forward directions. These disparities collapsed to simple vertical disparities in the projective binocular image plane. Subjects were able to perfectly fuse the vertically disparate target images with respect to the projected Helmholtz point of single binocular vision, independent of the particular location relative to the horizontal plane of regard. Target image fusion was achieved by binocular torsion combined with corrective modulations of the differential half-vergence angles of the eyes in the horizontal plane. Our findings support the notion that oculomotor control combines vergence in the horizontal plane of regard with active torsion in the frontal plane to achieve fusion of the dichoptic binocular target images.

DOI: https://doi.org/10.1152/jn.00596.2016

Three-dimensional ocular kinematics underlying binocular single vision

Bernhard J. M. Hess and H. Misslisch

Department of Neurology, University Hospital Zurich, Zurich CH-809, Switzerland

Abbreviated title: Binocular single vision

Corresponding author:

Dr. Bernhard J.M. Hess
Neurology Department
University Hospital Zurich
Frauenklinikstrasse 26
Zurich CH-8091

Phone: +41-1-255-5500
Fax: +41-1-255-4533
E-mail: bhess@neurol.uzh.ch

Abstract

We have analyzed the binocular coordination of the eyes during far-to-near re-fixation saccades based on the evaluation of distance ratios and angular directions of the projected target images relative to the eyes' rotation centers. By defining the geometric point of binocular single vision, called Helmholtz point, we found that disparities during fixations of targets at near distances were limited in the subject's three-dimensional visual field to the vertical and forward directions. These disparities collapsed to simple vertical disparities in the projective binocular image plane. Subjects were able to perfectly fuse the vertically disparate target images with respect to the projected Helmholtz point of single binocular vision, independent of the particular location relative to the horizontal plane of regard. Target image fusion was achieved by binocular torsion combined with corrective modulations of the differential half-vergence angles of the eyes in the horizontal plane. Our findings support the notion that oculomotor control combines vergence in the horizontal plane of regard with active torsion in the frontal plane to achieve fusion of the dichoptic binocular target images.

Key words:

Eye movements, Donders' law, Listing's law, dis-conjugate saccades, stereoscopic vision

New & Noteworthy

By defining the geometric point of binocular single vision, we found that disparities during fixations of targets at near distances were limited in the subject's three-dimensional visual field to the vertical and forward directions. These disparities collapsed to simple vertical disparities in the projective binocular image plane. We provide experimental evidence that ocular torsion supplemented by differential modulations of the half-vergence angles enables the fusion of saccadic targets in the near binocular visual field.

Introduction

For achieving binocular single vision precise coordination of eye positions is crucial. From a behavioral viewpoint two basic oculomotor constraints facilitate the coordination of the eyes during visually-guided movements in far vision. The first is that the eyes synchronously rotate in mutually parallel planes, which helps to keep the gaze lines in parallel alignment. More specifically, when the eyes move from a position straight ahead towards a target of interest at optical infinity both the direction straight ahead and the gaze line of each eye define planes, which are mutually parallel. That saccades move in planes has not only been shown for horizontal but also for vertical and oblique saccades (van Gisbergen et al 1985; King et al 1986; Dean et al 1999). The second is a consequence of the fact that the eyes' rotation planes are always chosen such that the torsional orientations of the retinae remains invariant with respect to straight ahead (assuming the head is still), irrespective of the order of ocular rotations. The particular rotation planes involved in these movements are known as direction-planes and the trajectories followed by the endpoints of each visual axis of an imagined fixed length as direction-circles (Helmholtz, 1867; Hess 2013; Hess and Misslisch 2015). Both geometric characteristics taken together facilitate binocular vision by reducing the complexity of the visual system's task to match corresponding features of the right and left retinal images, a problem often referred to as stereo correspondence problem (see for example Henriksen et al 2016). In different guise these properties are consequences of Donders' law extended to binocular vision (Donders 1848). It states that the ocular orientation during fixation of a particular target does not depend on the location of a previously fixated target whatever path the eyes may take in the configuration space of rotations.

Since these geometric constraints reduce the complexity of ocular configurations by keeping torsion invariant they represent a fundamental basis for the brain's task of matching corresponding features of retinal images. An additional benefit is that visual self-orientation is not affected by the order by which an observer scans the visual surround by saccades. Indeed, if ocular torsion would change depending on the saccade-order it would challenge the percept of a stationary visual surround. In fact, the retinal images might jump by several degrees relative to straight ahead while keeping the head still during the saccades[1]. Obviously, the distinction between object- and self-motion is more difficult in a perceived visual world with three rather than just two rotational degrees of freedom. In the near binocular fixation space, these problems become more acute for one thing because there is the freedom to choose the depth plane of fixation, for another, because binocular fixations require in general combining

[1] A 25° horizontal saccade followed by a 20° vertical saccade results in torsion of the retinal image of +4.5° compared to -4.5° if the saccade order is reversed.

vertical rotations in non-parallel direction-planes with rotations in the frontal plane (Mok et al 1992, van Rijn and Van den Berg 1993, Minken and van Gisbergen 1994). These complex compound rotations play a role in stereoscopic vision (Schreiber et al 2001), which suggests that they cannot be understood simply as passive consequences of the underlying ocular kinematics. Indeed, recent analyses of the kinematics of far-to-near re-fixation saccades have revealed that horizontal-vertical rotations during vergence eye movements were accompanied by a coarse ocular torsion, followed by a more fine-tuned torsion after some delay. Interestingly, neither of these torsions resulted from a Helmholtz-type of ocular kinematics as long believed. In contrast, these torsions must have been actively intended to supplement the default Donders-Listing kinematics in near vision (Hess and Misslisch 2015).

Although the geometry underlying the ocular kinematics in far vision suggests that fusion of near targets is not possible without ocular torsion it had been difficult to provide direct quantitative evidence. On the contrary, it has been widely believed that visual targets at finite viewing distances above or below the horizontal plane of regard[2] cannot be fused such that their images fall on non-corresponding retinal locations unless these targets lie in the midsagittal plane (Schreiber et al 2006). Accordingly, the locus of corresponding retinal points for converged eye positions (without torsion) has been defined as the projection of a single line orthogonal to the visual plane, i.e. to the horizontal plane of regard as defined in Fig. 1, in the midsagittal plane (vertical line horopter, see Helmholtz 1867, Howard and Rogers 1995). A geometric analysis of the binocular fixation space, however, shows that from an oculomotor viewpoint the eyes' visual axes can perfectly meet at positions defined by the intersection of two shells that can be drawn around each eye with the respective eye-to-target distances as radii. The locus of these particular target positions is a circle, here called Helmholtz circle for short (Fig. 1, circle 'h-h'). In order to focus on any point on the Helmholtz circle, the eyes have to rotate not only in vertical planes but also in the frontal plane, except for those singular positions, which correspond to intersections of the Helmholtz circle with the horizontal plane of regard. The torsional rotations move the disparate vertical Donders-Listing positions along minor circles until they meet each other at the Helmholtz circle. Since the required ocular torsions are generally quite small, they depend critically on the geometric location of the target of interest with respect to the eyes' rotation centers. In fact, it seems almost impossible to assess the relevant geometry with the appropriate accuracy and precision in view of the fact that the visual axes typically cross slightly in front or behind the geometric location of the target of interest, a phenomenon that has been called fixation

[2] The horizontal plane of regard is naturally defined as the plane spanned by the ocular rotation centers of the right and left eye and a fixation point at the horizon straight ahead with the head upright.

disparity (Schor 1980; Jainta et al 2015). An evaluation of the order of magnitude of fixation disparities, which depend on both the inter-ocular distance and the difference between target and actual fixation distances (Howard and Rogers, 1995) shows that misestimating these parameters in the range of per mill would result in disparities in the arc-second range. Since the acuity of stereoscopic vision lies in the range of arc seconds (Badcock and Schor 1985, Schumer and Julesz 1984; Westheimer 1979), an evaluation of the actual fixation geometry at this level of accuracy appears to be out of practical reach. Confronted with this problem we were looking for a different approach to quantify oculomotor coordination during fixation of targets in near visual space.

In an attempt to solve this problem we aimed at answering the following two closely related questions: First, what are the relevant parameters for estimating the binocular location of a target in near fixation space? Second, what are the oculomotor principles that underlie the binocular coordination of the kinematics during fixation and fusion of targets in the near visual space? To answer these questions we studied far-to-near re-fixation saccades in rhesus monkeys using a simple algorithm that allows a precise quantitative assessment of the binocular coordination of the eyes. The algorithm was evaluated on data that have been obtained from three behaviorally trained rhesus monkeys, which earlier have served as subjects in a related three-dimensional (3D) kinematics study (Hess and Misslisch 2015). Here we present evidence that it is indeed ocular torsion, supplemented by small corrections of the vergence angle, that enables perfect fusion of near targets in the binocular visual space that otherwise would not be possible at locations off the horizontal plane of regard.

Materials and Methods

The experimental data were obtained from three female rhesus monkeys (*Macaca mulatta*), which had a chronic acrylic head implant for restraining the head in the experimental sessions. Three-dimensional eye movements were recorded with the magnetic search coil technique (Robinson 1963) using a dual search coil that was implanted on both eyes under the conjunctiva as previously described (Hess 1990, Mandelli et al 2005). All surgery was performed under aseptic conditions and general anesthesia, and postoperative pain treatment was applied for at least three consecutive days. All procedures were in accordance with the recommendations in the Guide for the Care and Use of Laboratory Animals of the US National Institutes of Health. The housing, husbandry and experimental procedures were reviewed, approved and supervised by the Veterinary Office of the Canton of Zurich.

Experimental procedures

The animals were trained to re-fixate between a far and a near light-emitting diode. The far target was located at eye level 0.8 m straight ahead (horizontal vergence ~2°, vertical eye position ~0°). The near target was located 10° down at a distance of 0.1 m (horizontal vergence 17°). To examine a larger range of azimuth and elevation angles including asymmetric vergence effects we analyzed in a first step all saccades that landed on or in the vicinity of the near target. In a second step, we excluded those trials, which did not fulfill the fusion criteria as explained in the result section. All experiments were performed in dimmed light, i.e. with a background illumination inside an opaque sphere where the animal was seated upright, with the head restrained in a primate chair, which completely surrounded the animal. Three-dimensional eye positions were recorded with an Eye Position Meter 3000 (Skalar, Delft, The Netherlands) , calibrated as described in Hess et al. (1992), digitized at a sampling rate of 833.33 Hz, and stored on a computer for off-line analysis. To express eye positions as rotation vectors (Haustein 1989), the zero or reference positions were defined to be the eye's orientations while the monkey fixated a target 0.8 m straight ahead. In two animals (M1, M2), Listing's plane tilted less than -2° vertically and -1° horizontally, in one animal it tilted vertically about -6° and horizontally 0° (M3). We did not correct eye positions for these deviations from primary position (see Hess and Thomassen 2014). The on- and offset of saccades were isolated by a semiautomatic procedure based on the magnitude of the jerk (derivative of angular eye acceleration), followed by applying an empirically adjusted position threshold based on the relative change in magnitude of the eye position vector (Hess 2013). Specifically, after choosing a position threshold in the one-figure percent range the time course of the coarsely delimited saccadic events was narrowed down to stay within these provisional limits (where they exceeded the threshold). To further refine the saccade window, we computed the mean +SD of the initial rising phase up to the point of exceeding the threshold, which determined the final onset-threshold. Likewise we computed the mean +SD of the falling phase below threshold, which defined the final offset-threshold of the saccade. This procedure avoids noise problems inherent with velocity or acceleration thresholds and isolates saccades by preserving their typically asymmetric time course. Saccades with amplitudes < 1° were discarded.

Vectors will be denoted by bold characters, unit vectors by regular fonts with caret. When referring to components, we write vectors for convenience as row vectors within round parentheses, separating the components by commas.

Gaze movements and representation of 3D eye position

3D eye positions were represented in the convenient axis-angle representation of rotation vectors, where the magnitude of rotation is expressed as tangent of half the angle of rotation (ρ), and the axis as a vector of unity length orthogonal to the plane of rotation (denoted $\hat{n}$): $\boldsymbol{E} = \left(E_{tor}, E_{ver}, E_{hor}\right) = \tan(\rho/2)\hat{n}$ (Haustein 1989). Torsional eye position, E_{tor}, is the rotation of the eye in the head's frontal plane (in subject's view clockwise positive), vertical eye position, E_{ver}, is the rotation in the vertical plane (downward positive), and horizontal eye position, E_{hor}, is the rotation in the horizontal plane of regard containing the reference position straight ahead (leftward positive).

To relate gaze shifts in visual space to the underlying rotations of the eye, we represented the gaze line by a unity vector, $\hat{g} = \sum_{i=1}^{3} g_i \hat{e}_i$ in the spherical field of fixations with coefficients $g_1 = \cos\varepsilon$, $g_2 = -\sin\varepsilon\sin\psi$ and $g_3 = \sin\varepsilon\cos\psi$ using the polar coordinate ε, describing the angular eccentricity relative to straight ahead and ψ, the signed dihedral angle between the plane $\hat{e}_1 \times \hat{g}$ and the mid-sagittal plane represented by $\hat{e}_1 \times \hat{e}_3$ (right side down positive)[3]. The unit vectors $\hat{e}_i$ (i =1, 2 and 3) represented a right-handed, head-fixed Cartesian coordinate system with $\hat{e}_1$ pointing in direction straight ahead, $\hat{e}_2$ pointing along the inter-ocular line from right to left, and $\hat{e}_3$ pointing upward (Fig. 2). A general rotation of the eye was described by a rotation operator $R = R(\hat{n}, \rho)$, where the unit vector $\hat{n}$ describes the orientation of the rotation plane and ρ the angle of rotation. A rotation of the gaze vector from A to B in the plane $\hat{n}$ through the angle ρ is obtained by the operation $\hat{g}_B = R_{BA}\hat{g}_A R_{BA}^{-1}$, where $R_{BA}^{-1} = R_{AB}$ is the inverse of R_{BA}.

To assess the cyclovergence during far-to-near re-fixation saccades we needed to segregate ocular torsion from the Donders-Listing rotation of the eye. This can be done by reconstructing the Donders-Listing rotation, from which the rotation in the frontal plane, denoted R_F is obtained by solving the equation $R_{\exp} R_{DL}^{-1} = R_F$ (Hess and Misslisch 2015). Here we used the inverse approach, in which first the overall torsion of the eye was determined. The Donders-Listing rotation was then obtained from the equation $R_F^{-1} R_{\exp} = R_{DL}$.

---

[3] In geometric terms the cross product of two unit vectors, $\hat{e}_i \times \hat{e}_j$ (i ≠j) represents an oriented unit plane. Indeed the exterior product (bi-vector) $\hat{e}_{ij} = \hat{e}_i \wedge \hat{e}_j$ is related to the cross product by $\hat{e}_i \times \hat{e}_j = -(\hat{e}_i \wedge \hat{e}_j)\hat{e}_{123}$, using the 3-dimensional pseudo-scalar $\hat{e}_{123} = \hat{e}_1\hat{e}_2\hat{e}_3$.

In this approach no assumption is made about the specific direction-plane of rotation of the Donders-Listing rotation.

Segregation of torsion from the recorded experimental rotation

Having measured the overall rotation of the eye, denoted by R_{exp}, we determined the torsion by the following ansatz:

$$R_{\text{exp}} = R_F(\xi)\, R_{DL}(\rho)$$

Here the first rotation is a Donders-Listing rotation (R_{DL}) in an unknown direction-plane through an angle ρ. The subsequent rotation is a rotation in the frontal plane (called ocular torsion) through an angle ξ. The unknown torsional angle ξ was obtained by evaluating the scalar products $\langle R_{\text{exp}}, I\rangle$ and $\langle R_{\text{exp}}, \hat{\gamma}_{23}\rangle$, which yield the two relations $u_0 = \langle R_{\text{exp}}, I\rangle = \cos\xi/2\cos\rho/2$ and $u_1 = \langle R_{\text{exp}}, \hat{\gamma}_{23}\rangle = -\sin\xi/2\cos\rho/2$.[4] The rotation angle ξ in terms of u_0 and u_1 thus is $\xi = -2\sin^{-1}\left(u_1/\sqrt{u_0^2+u_1^2}\right)$, with $\sqrt{u_0{}^2+u_1{}^2} = \cos\rho/2$. The Donders-Listing rotation R_{DL} associated to R_{exp} was thus $R_{DL} = R_F^{-1}(\xi)\, R_{\text{exp}}(\rho)$.

With the Donders-Listing rotation R_{DL} at hand we analyzed the fixation positions of the eyes before and after the intervention of ocular torsion. For this we used the property of commutativity for factorizing eye positions into conveniently parameterized Donders-Listing rotations (for a proof of commutativity, see Appendix). First we compared R_{DL} to the following torsion-free compounded rotation $R_{DL} = R_v(\eta)\, R_H(\vartheta)$ where the first rotation, denoted R_H is a rotation in the horizontal plane of regard through the azimuth ϑ and the second rotation, denoted R_v is a rotation in the vertical-direction plane through the angle η. To solve this equation for ϑ, we computed the scalar products $v_0 = \langle R_v R_H, I\rangle = \cos\eta/2\cos\vartheta/2$ and $v_3 = \langle R_v R_H, \hat{\gamma}_{12}\rangle = -\cos\eta/2\sin\vartheta/2$, from which we obtained $\vartheta = -2\sin^{-1}\left(v_3/\sqrt{v_0^2+v_3^2}\right)$ and $\eta = 2\cos^{-1}\left(\sqrt{v_0^2+v_3^2}\right)$. The angle η thus was the angle through which the eye would have to rotate in the vertical-direction plane to reach the respective position given by R_{DL}.

To determine the dihedral angle ψ as a function of ocular eccentricity, we solved the

---

[4] Definition of the Clifford scalar product: The Clifford scalar product of x and y, denoted by $\langle x, \mathrm{y}\rangle = \left(xy^{\dagger}\right)_0$ is the coefficient of the unity I of the Clifford product $xy^{\dagger}$ where $y^{\dagger}$ is the reverse of y (see Snygg 1997).

equation $R_{DL} = R_M(\eta)$ where R_M represented a meridian rotation in the plane ψ =constant. From the two scalar products $m_2 = \langle R_M, \hat{\gamma}_{31} \rangle = \sin(\mu/2)\cos\psi$ and $m_3 = \langle R_M, \hat{\gamma}_{12} \rangle = \sin(\mu/2)\sin\psi$, we obtained the dihedral angle $\psi = \sin^{-1}\left(m_3 / \sqrt{m_2^2 + m_3^2}\right)$ and the rotation angle $\mu = 2\sin^{-1}\sqrt{m_2^2 + m_3^2}$ in the meridian plane (for more details of these calculations, see Appendix).

With the azimuths of the Donders-Listing positions of right and left eye we defined the differential half-vergence angles $\delta\alpha = \alpha - \alpha_{DL}$ and $\delta\beta = \beta - \beta_{DL}$ of the right and left eye. Here and in the following α, β denote the half-vergence angles of R_{exp} and α_{DL} and β_{DL} the azimuths associated to the Donders-Listing positions. We compared these angles with the ω-torsion of the right and the left eye, which we have earlier defined as the difference between the ocular torsion at the fixation point and the associated Donders-Listing position (Hess and Misslisch 2015: see Fig. 4B).

Binocular coordination of fixation points

In binocular visual space the location of a saccadic target can be conceived as the vertex of a triangle with baseline joining the two rotation centers (Fig. 3B, triangle O_a O_b A). In general there are two such slightly incongruent triangles, one associated to the right eye and one associated to the left eye. The projective images of fixation triangles on the retina are again triangles except for fixations in the horizontal plane of regard. In general these triangles are slightly incongruent, spanning different planes (Fig. 3B, top view on triangles $O_aO_bA_a$ and $O_aO_bA_b$, formed by the common base line O_aO_b and the right (O_aA_a) and left gaze line (O_bA_b), respectively), except in cases where their vertices coincide with a Helmholtz point (Fig. 3B, triangle O_aO_bA). Since dichoptic fixation positions must lie on the respective direction-circles both above or below the horizontal plane of regard (see white circles in Fig. 1A) they can always be brought into coincidence by appropriate torsions of the right and left eye. Since ultimately we are interested in the retinal images, we focus the subsequent geometric analysis on the plane orthogonal to the horizontal plane of regard, which we call the principal plane (Fig. 3A).

We denote the distances between the rotation centers and the fixation point A by $a = \left\|\overrightarrow{O_aA}\right\|$ and $b = \left\|\overrightarrow{O_bA}\right\|$, respectively. Similarly, we define the inter-ocular distance D as the

distance between the two rotation centers $D = \left\| \overrightarrow{O_a O_b} \right\|$ (Fig. 2 C). Based on the proportion[5] $a/b = \cos\beta/\cos\alpha$, where α and β are the azimuths of the right and left eye, respectively, we have the following geometric relations between the triangular base of length D, the two sides of lengths a, b and the azimuth angles α, β (Fig. 3B):

$$D = \mathrm{a}\cdot\sin\alpha - \mathrm{b}\cdot\sin\beta$$
$$a = D\cos\beta/\sin(\alpha-\beta) \qquad (1)$$
$$b = D\cos\alpha/\sin(\alpha-\beta).$$

The locus of visual positions 'A' that subtend a constant angle at the centers of rotation without changing azimuth is a circle generated by rotating the vertex A about the baseline (circle h-h in Fig. 3A). We refer to this circle as Helmholtz circle of binocular single positions (Hess and Misslisch 2015). In the spherical visual field, the Helmholtz circle is the intersection of two shells of fixation positions at constant distances from the respective rotation centers (shells denoted by T_a, T_b in Fig. 3A). To study the fixation positions during saccades, we described the gaze line of the right and left eye by the time-dependent vectors $\boldsymbol{g}_a = a\hat{g}_a, \boldsymbol{g}_b = b\hat{g}_b$, where $\hat{g}_a = \hat{g}_a(t)$, $\hat{g}_b = \hat{g}_b(t)$ were unit vectors describing the spatial directions and the scalars a =a(t), b =b(t) were the lengths of the vectors $\boldsymbol{g}_a$, $\boldsymbol{g}_b$, representing the distances of the fixation points with respect to the rotation centers O_a and O_b as a function of time. However, since distance is not an invariant in the projected retinal images of the eyes, we used distance ratios based on the proportions $a:D = a':1$ and $b:D = b':1$, which imply that D =1 in equations 1 (Fig. 4). In the following we rename the side lengths a´ and b´ of the normalized triangle a and b for notational simplicity, referring to them as fixation distances. It should be noted that equations (1) and the thereof derived distance ratios were robust against variability of the relative location of the rotation centers in a frequency range of up to a few hundred Hertz because of the sampling rate used to record the azimuth angles α and β during the saccades. In general, the position vectors $\boldsymbol{g}_a$, $\boldsymbol{g}_b$ of the eyes define disparate fixation points. In the Cartesian coordinate system used, we place the rotation center of the right eye, labelled O_a at the origin and that of the left eye O_b at a distance of 1 from O_a on the y-axis (horizontal axis). The Helmholtz circle, projected onto the principal plane, partitioned the unitary inter-ocular segment $I = [0\ 1]$ by the vertical line joining the two points of intersection

[5] This is the sine law for a triangle with side lengths 1, a, b and angles $\alpha' = \pi/2 - \alpha$ opposite to side b and $\beta' = \pi/2 - \beta$ opposite to side a.

of the iso-eccentricity circles as follows (Fig. 3): $I = I_a + I_b = H_y + \left(1 - H_y\right)$, where $H_{\pm} = \left(0, H_y, \pm H_z\right)$ denoted the two intersection points, called Helmholtz points. Notice that the coordinate H_y of $H_{\pm}$ may lie in between or to either side of the rotation centers on the y-axis.[6] To characterize the vergence angle, we computed the angle γ subtended by the two rotation centers at the fixation points in the binocular visual field as follows

$$\gamma = \alpha - \beta = \sin^{-1}\left(I_a/a\right) - \sin^{-1}\left(I_b/b\right), \tag{2}$$

where α, β are the angles subtended by the intervals I_a and I_b, respectively.[7] For version eye movements (with the gaze lines parallel) the angle γ vanishes because fixation is at infinity, whereas in near space the angle γ increases with decreasing fixation depth. It should be emphasized that equation 2 also holds in the general case when the gaze lines are not in the horizontal plane of regard and do not necessarily meet at a single position in the binocular visual field (see A_a and A_b in Fig. 3B). In this case, the fixation points of the right and left eye lay at disparate vertical positions in a plane parallel to the Helmholtz circle. Denoting the fixation points of the right and left eye by A_a, A_b, and their projections onto the principal plane by A'_a, A'_b, we computed the angles subtended by the segments $O_a A'_a$ and $O_b A'_b$ at the fixation points as follows (Fig. 3C, projections A′, A'_a, A'_b not displayed)

$$\boldsymbol{F}_a = \tan^{-1}\left(\left[\hat{g}_a\right]_{x=0} / \left[\hat{g}_a\right]_x\right), \boldsymbol{F}_b = \tan^{-1}\left(\left[\hat{g}_b\right]_{x=0} / \left[\hat{g}_b\right]_x\right), \tag{3}$$

where $\left[\hat{g}_a\right]_{x=0} = \hat{g}_a\left(0, y, z\right)$, $\left[\hat{g}_b\right]_{x=0} = \hat{g}_b\left(0, y, z\right)$ are the projections of the vectors $\hat{g}_a$, $\hat{g}_b$ onto the principal plane; $\left[\hat{g}_a\right]_x$, $\left[\hat{g}_b\right]_x$ denote the x-component of $\hat{g}_a$, $\hat{g}_b$. The 2D vectors $\mathbf{F}_a$ and $\mathbf{F}_b$ represented the angular direction and eccentricity of the images of the fixation points in the principal plane. To determine the unique position admitting binocular single vision, we computed the intersection of the iso-eccentricity circles with radii $r_a = \left\|\boldsymbol{F}_a\right\|$ and $r_b = \left\|\boldsymbol{F}_b\right\|$, centered at the respective rotation centers O_a and O_b. In general there are two intersection points which lie on the projected image of the Helmholtz circle. To avoid confusion with fixations points, we denoted these two intersection points in the projection plane by H'_+ and H'_- (Fig. 3A, C, D).

[6] Since we considered only convergent fixations, the positions lay all in front of the subject.
[7] These definitions are independent of the length of the inter-ocular distance because both a, b are distance ratios; they scale with the inter-ocular distance k.

Oculomotor fixation disparity

All points on the projected image of the Helmholtz circle between and including the points H'_+ and H'_- represent corresponding retinal points (see Discussion). To determine the disparity between the points A'_a and A'_b on one hand and the closer of H'_+ and H'_- on the other, we computed the angular differences with respect to the rotations centers O_a and O_b by

$$\delta y_a = \left|\left[\boldsymbol{F}_a\right]_y - \left[\boldsymbol{H}_a\right]_y\right| = -\delta y_b = \left|\left[\boldsymbol{F}_b\right]_y - \left[\boldsymbol{H}_b\right]_y\right| \qquad (4)$$

$$\delta z = \left|\left[\boldsymbol{F}_a\right]_z - \left[\boldsymbol{F}_b\right]_z\right|$$

Here, $\boldsymbol{H}_a = \left(\left[\boldsymbol{H}_a\right]_y, \pm\left[\boldsymbol{H}_a\right]_z\right)^T$ and $\boldsymbol{H}_b = \left(\left[\boldsymbol{H}_b\right]_y, \pm\left[\boldsymbol{H}_a\right]_z\right)$ denote the position vectors of the Helmholtz points relative to O_a and O_b, respectively. Similarly, we computed the disparity of the associated Donders-Listing positions by

$$\delta y'_a = \left|\left[\boldsymbol{D}_a\right]_y - \left[\boldsymbol{H}_a\right]_y\right|, \delta y'_b = \left|\left[\boldsymbol{D}_b\right]_y - \left[\boldsymbol{H}_b\right]_y\right|, \ \delta z' = \left|\left[\boldsymbol{D}_a\right]_z - \left[\boldsymbol{D}_b\right]_z\right| \qquad (5)$$

where $\mathbf{D}_a$ and $\mathbf{D}_b$ denote the position vectors of the respective Donders-Listing position relative to O_a and O_b. Because the fixation points were located on the same iso-eccentricity circle in close vicinity to the Helmholtz point, the vertical disparities are expected to linearly depend on the horizontal fixation disparity. Therefore we fitted the vertical disparities as a function of horizontal fixation disparities by a straight line $\delta z = p\delta y + q$ using the method of minimal least squares and computed the coefficient of variation (Anderson-Specher 1994). The interceptions of the fitted straight line with the y- and z-axis provided the offsets of the subject's average estimation of target location in 3D binocular fixation space.

In an attempt to quantify target fusion, we measured the surface of the triangle spanned by the Helmholtz point and the fixation points A_a and A_b (Fig. 3B, shaded triangle A_aA_bA). We used Heron's formula, which expresses the area of the triangle as a quadratic function of the side lengths. Earlier kinematic analyses of re-fixation saccades suggested that the fusion of targets off the horizontal plane of regard required ocular torsion (Hess and Misslisch 2015). Since this would reduce the vertical disparity as a quadratic function of the horizontal fixation disparity, we fitted the triangle areas by a parabolic function of the horizontal fixation disparities, $S = u\delta y^2 + v\delta y + w$ and computed the coefficient of determination.

Results

Triangulation of fixation positions in binocular fixation space

Based on the derived fixation distances and directions (see equations 1), we computed the angles subtended by the arcs joining the rotation centers to the projected images as viewed at the fixation points in space. The metrics used in the principal plane thus was 2D angular distances and directions of the projected fixation points relative to respective rotation centers. Depending on the relative distances to the visual scene, the projected fixation points exhibited vertical but not horizontal disparity (Fig. 5). This vertical alignment was a consequence of equation 1. Since this equation describes each eye's fixation triangle by a common baseline and the eye's visual axis the respective triangles must be congruent, i.e. of same size and shape, but not necessarily sharing the same position in 3D space. Specifically, they can be rotated relative to each other by means of a rotation about the common baseline O_aO_b. Thus, in the general case these triangles do not span a common plane and therefore project onto incongruent triangles in the principal plane (compare triangles spanned by $O'_aO'_bA'_a$ and $O'_aO'_bA'_b$ in Fig. 5C, D). By the same token the fundamental constraint $1 = I_a + I_b = a\sin\alpha - b\sin\beta$ of binocular coordination restricts the possible disparities between the eye's fixation points to the vertical and forward (depth) direction. Notice that this constraint holds also for points off the horizontal plane of regard by virtue of the two relations $\sin\alpha = -\sin\psi_a \sin\varepsilon_a$ and $\sin b = -\sin\psi_b \sin\varepsilon_b$ (see also Discussion, Appendix).[8]

Far and near fixation points and Donders-Listing positions

The fixation positions at the onset of saccades differed generally little from the respective Donders-Listing positions as long as the saccade onset positions were close to optical infinity. In near vision, however, these positions clearly segregated from the fixation points (Fig. 6, compare A with B). To analyze the geometry underlying this segregation we aligned the fixation points of saccades with the vertical axis in the principal plane. This transformation clearly segregated the Donders-Listing positions from the fixation points (Fig. 6C). According to kinematic analyses we knew that each of these positions should be located on the iso-eccentricity circle associated to the respective fixation point. To test this prediction we plotted the iso-eccentricity circles through the fixation points using the transformation $y' = y - y_{FP}$ where y_{FP} denoted the horizontal coordinate of the fixation point, leaving the vertical coordinates unchanged (Fig. 7 A, B). We found that the Donders-Listing positions

[8] Notice that the eccentricity angles ε_a and ε_b of the two points converge towards the half-vergence angles α and β for both $-\psi_a$ and ψ_b converging towards $\pi/2$.

indeed very accurately lay on the respective iso-eccentricity circles. To quantify these observations, we measured the radial distances of the Donders-Listing positions with respect to the rotation centers and compared them to those of the respective iso-eccentricity circles through the fixation points. Specifically, we measured the absolute difference between the Donders-Listing (R_{DL}) and fixation radii (R_F) and expressed the variability by the ratio $\delta\rho = \left|R_{DL} - R_F\right| / R_F$. In the subject illustrated in Fig. 7, we found average ratios across the last 100 ms of the saccade of 2.9 (±3) x 10^{-5} for the right eye and 1.1 (±1.1) x 10^{-4} for the left eye (N =25 x 83, trials times sample points in a single session). The projected fixation positions in the principal plane, average vergence angles, target shell radii and variability of eccentricity radii are summarized Table 1 and 2 for all subjects and experimental sessions.

As earlier reported, the rotation from Donders-Listing positions to the fixation position requires fined-tuned torsion, called ω-torsion to distinguish it from the overall coarse torsion of the eyes during the re-fixation saccades (Hess & Misslisch 2015). In the following paragraph we address the question of how accurately this torsion aligns the eyes' final position with the binocular single position predicted by the binocular algorithm. We refer in the following to both the binocular single position in fixation space (i.e. geometric meeting point of gaze lines) as well as to its projected image in the principal plane as Helmholtz point.

Visuo-motor fixation disparities

We measured the angles that the arcs joining the projected images of the fixation and Helmholtz points subtended at the fixation points in the visual fixation space (see equation 4, Methods). Since these angles represented angular differences relative to the Helmholtz point we referred to them as fixation disparities or simply disparities. Notice that the term 'horizontal disparity' always refers to the disparity relative to the Helmholtz point whereas the term 'vertical disparity' refers to the mutual disparity between the fixation points. Using an analogous procedure we compared these fixation disparities with those of the associated Donders-Listing positions (see equation 5, Methods). Since there are many reasons for missing or inappropriate target fusion at the end of a saccade we used the two following criteria for deciding whether the subjects did make a successful attempt to fuse the near target. First, we required that the average absolute value of the vertical disparities of the fixation points and the Donders-Listing positions were different from each other at the significance level p=0.05 or smaller. Second, we required that the mean of the absolute vertical disparities of fixation positions was smaller than that of the corresponding Donders-Listing positions. Because the fixation positions exhibited no horizontal disparities these two criteria are necessary conditions for the occurrence of a partial or full fusion of the target. The disparities

found following these criteria are summarized in Table 3 for each animal and experimental session. In some sessions only part of the trials fulfilled the criteria as indicated. We discarded all data, which did not fulfill the fusion criteria.

Because the horizontal disparities of the fixation points differed only in sign, the graphs showing vertical versus horizontal disparities were symmetric with respect to the z-axis. For clarity we reflected the right eye's fixation points and the Donders-Listing positions at the vertical axis through zero (see the example in Fig. 8B, first row). To obtain an estimate of the average disparity relative to the Helmholtz point, we measured the offsets of the best-fitted straight lines $\delta z = p\delta y + q$ to the vertical (δz) versus horizontal disparities (δy) in the principal plane. We found that these fits predicted with high accuracy the location of the Helmholtz point (Table 3; Fig. 8A). Offsets, slopes and coefficients of determination are summarized in Table 4. Altogether these data suggested that fusion or partial fusion of targets occurred across a range of vertical disparities of up to about 1°.

To further quantify the fusion process we computed the surface of the projected triangles outlined by the fixation and associated Helmholtz points (see Fig. 3B, shaded triangle A_aA_bA). As expected the area of the fusion triangles increased with increasing horizontal disparity in a non-linear fashion (Fig. 8C). For each experimental session, we fitted the areas as a function of horizontal disparities with a parabola. Due to the vertical alignment of the fixation points (i.e. the zero horizontal disparity), we reflected the data on the vertical through the Helmholtz point such that the vertex of the fitted parabola fell on this line. Accordingly the vertical offset of the vertex provided an estimate of the minimal fusion area that can be extrapolated from the actual fixation positions (Fig. 8C). Averaging these areas across sessions, we found extrapolated fusion areas of 0.005 (0.008) arc min square in M1 (R^2=0.99 (0.02), N=63), 0.008 (0.015) arc min square in M2 (R^2=0.98 (0.03), N=229), 0.0 ($1.5\cdot10^{-4}$) arc min square in M2* (R^2=1.0 (0.004), N=20), and $2.7\cdot10^{-4}$ arc min square in M3 (R^2=0.96, N=19). For comparison, the actual fusion areas (±SD) calculated by using Heron's formula are summarized for far and near fixations in Table 4. In contrast to the final fixations, the geometric pattern of the associated Donders-Listing positions showed in general no correlation of the triangular areas with horizontal disparity. One reason for this was that these patterns were often not symmetric relative to the vertical axis but shifted and rotated towards one or the other side (Fig. 8B). Taken together these observations suggested that the torsion of the eyes was not the only rotation that contributed to target fusion. Rather motor target fusion was achieved through compounded rotations in the frontal and horizontal plane as shown in more detail in the subsequent paragraph.

Differential vergence and ω-torsion

Although the ω-torsion of the eyes was instrumental in achieving target fusion in near vision, a comparison of the geometric patterns of Donders-Listing positions before fusion to those of the fixation points suggested that torsion was not the only motor action during the process of target fusion. Since the ω-torsion was more or less symmetric one would have expected that the modulation of the eye's half-vergence angles would reflect a similar symmetry if it were exclusively the consequence of the ω-torsion of the eyes. This was not the case since we found that the modulations of the differential half-vergence angles (defined in Methods) were not only asymmetric compared to the respective ω-torsion but also sometimes showing significantly earlier onsets (Fig. 9).

Discussion

We have analyzed the binocular coordination of the eyes during saccadic re-fixations across the visual field. Since Euclidean distances are not preserved in the visual percept, we based our analyses on angular directions and distance ratios of the projected retinal images. Under these premises, the evaluation of binocular coordination of far-to-near re-fixation saccades yielded three major findings: First, on pure geometrical grounds, the fixed lateral separation of the eyes admits only disparities between the fixation points in vertical directions and in depth. Second, the horizontal disparity between the eyes' fixation points and the point of single binocular vision, the Helmholtz point, varied in the same experimental session between values close to zero, indicating full target fusion, up to about 1° allowing partial fusion. Third, partial or full target fusion was achieved by active torsions of the eyes, accompanied by modulations of the differential half-vergence angles in the horizontal plane of regard if necessary. Altogether, these findings strongly support the hypothesis that oculomotor control combines vergence in the horizontal plane of regard with torsion of the eyes in the frontal plane to fuse targets and achieve binocular single vision.

It has earlier been suggested that ocular torsion in near vision improves binocular image alignment by reducing retinal disparity (Tweed 1997; Schreiber et al 2001; Schreiber et al 2006). Here we showed that it is indeed the fined-tuned component of ocular torsion during the re-fixation saccade (ω-torsion, Hess-Misslisch 2015) in cooperation with a modulation of the differential half-vergence angles, which drive the fusion or partial fusion of the projected target in a binocular image plane (for a definition of the differential half-vergence angles, see Methods). While ocular torsion was necessary to enable target fusion on simple geometric

grounds, the differential modulation of the horizontal vergence allowed corrections for small asymmetries of gaze directions relative to the Helmholtz point (Fig. 9). We have earlier provided evidence that ocular torsion becomes necessary to compliment the Donders-Listing kinematics of the eye in order to enable binocular fusion of near targets located off the horizontal plane of regard. The reason for implementing this additional degree of rotational freedom of the eyes lies in the particular configuration of the direction planes defining the admissible vertical fixation directions during convergence. Although the gaze lines obviously always meet at a single point when the eyes converge in the horizontal plane of regard, they would always diverge above or below the horizontal plane, even in symmetric convergence. To overcome this shortcoming, the eyes must torque to enable fusion of near targets off the horizontal plane of regard (Hess and Misslisch 2015).

To quantify the process of fusion we defined disparity on one hand as vertical angular distance between the fixation points and on the other as horizontal angular distance between the vertically aligned fixation points and the Helmholtz point. We found that the fixation points always approached the Helmholtz point by moving along the converging iso-eccentricity circles with little scattering (Fig. 7B). Thus knowledge of the relative target distances and the mutual vertical disparity determined the horizontal disparity. By the same token we found that the parabolic fits of the fusion areas yielded vanishing linear coefficients and vertical offset (Fig. 8C). Implications of this finding with regard to the problem of scaling disparities in stereoscopic vision are addressed in the subsequent paragraphs.

Problem of scaling disparities

For assessing binocular coordination in the image plane, called principal plane in our model, the most natural choice of coordinates are polar angles that describe both angular target eccentricity and direction. More specifically, we based our evaluations on a description of the ratio of target eccentricity to target distance and angular directions relative to the locations of the projected ocular rotation centers in this plane. According to the lateral separation of the rotation centers, the half-vergence angles describing the observer's gaze direction in the horizontal plane of regard provided the only geometric link between the projection of the spherical fixation fields of each eye. We used the fact that these angles can in a simple way be related to the target coordinates in the principal plane on one hand and to the distance ratios in binocular fixation space on the other (see equations 1). In the vicinity of the estimated binocular single image of a target, the Helmholtz point, we found that horizontal fixation disparities and vertical disparities were linearly correlated. This was to be expected as long as the slopes of the circular iso-eccentricity segments defining the Helmholtz point were

finite. Thus, vertical disparities do locally provide no cues about the structure of the visual scene, except maybe for gauging fixations close to the horizontal plane of regard, where target fusion requires no ocular torsions (see later). On a global scale, however, horizontal and vertical disparities of the visual scenes are independent parameters involving the inter-ocular separation, the distance to a common fixation point as well as gaze direction. Based on such global parameterization it has been shown that the three-dimensional structure of the visual scene can be computed from a few image points (Mayhew, Longuet-Higgins, 1982; Frisby 1984; Bishop 1989; but see also: Cumming, Johnston and Parker 1991; Cumming 2002; Read and Cumming 2006).

The role of fixation positions in near target fusion

From an integrative visuo-motor standpoint, it is of interest to compare the process of re-fixation in far-to-near saccades with the process of stereoscopic depth perception as described by the concept of point horopter. First, it should be mentioned that the Helmholtz points defined by the intersections of iso-eccentricity circles in the principal plane or by the intersection of the target shells in the binocular fixation space (Hess and Misslisch 2015) coincide with positions on the point horopter as far as they can be reached by eye movements. In contrast, the fixation positions defining a specific fixation depth are lying on the respective iso-eccentricity circles, which deviate from the more curved point horopter (Fig. 10). The disparity gradient of fixation positions thus changes much less as a function of gaze direction than the gradient of the neighboring geometric corresponding points. The reason is that the fixation depth is typically much larger than the radius of the Vieth-Müller circle. Since binocular single vision ultimately depends on the binocular coordination of inherently dichoptic fixation positions it would be interesting to see whether these differences might contribute to the observations that the empirical horopter is less concave than the classical point horopter (Ogle 1964, Helmholtz 1867; Siderov et al 1999; Schreiber et al 2008). Indeed fixation-positions that might scatter along their iso-eccentricity arcs in the neighborhood of a Helmholtz point (arcs labelled ‘a-a’ and ‘b-b’ in Fig. 10) always straddle the horizontal point horopter. The depths differences associated with these dichoptic positions thus are in rivalry to the depth signature of iso-vergence positions. A perceptual consequence of this configuration thus might be Panum’s fusional area (Panum 1858, Fischer 1924). Additional depth cues can be gathered from the vertical neighborhood of the Helmholtz point, where the binocular visual surround is differently structured. For example, fixation points in the horizontal vicinity of a Helmholtz point that exhibit disparity in depth can segregate into vertically disparate fixation points when the gaze lines move out of the horizontal plane (see

A'_a, A'_b in Fig. 5). Exploiting such cues likely helps estimating stereoscopic depth. In fact, experiments with dynamic random dot stereograms have provided evidence that stereopsis can detect the depth of matches over a range of both vertical and horizontal disparities (Stevenson and Schor, 1997).

Fixation points and geometric corresponding points

The problem of quantifying retinal correspondence across changes in 3D eye positions has been recently discussed in the studies of Schreiber et al (2006, 2008), which show how the 3D shape of the empirical horopter depends on assumptions about the underlying kinematic model and fixation directions. Particularly interesting in this context is the asymmetry between the classical notion of corresponding retinal points in the horizontal plane of regard and its extension to the vertical visual field. The theoretical vertical horopter has been described as vertical line tangent to the point of symmetric convergence on the horizontal point horopter (Prévost 1843; Howard and Rogers 1995). Psychophysical studies have shown that the empirical vertical horopter is tilted (Helmholtz 1867; Nakayama 1977; Siderov et al 1999; Sprague et al 2015). Thus, in contrast to the horizontal point horopter none of the positions on the theoretical or empirical vertical horopter is accessible to fixation without changing both vergence and torsion of the eyes. It has been pointed out that the extension of the classical point horopter in vertical dimensions leads to ambiguities in the notion of corresponding retinal points (Schreiber et al 2005). Based on the motion patterns of far-to-near re-fixation saccades it appears that the subjects estimated the location of the near target by determining the Helmholtz point using equidistant or iso-eccentricity cues. In cases where the subject's saccade hit the near target in symmetric vergence head-on, the projection of the respective Helmholtz circle would fall on vertical corresponding retinal points such that horizontal disparities are bound to provide reliable cues for estimating the depth of the target. Alternatively, if the subject initially was looking to the side such that the estimated target location would be in asymmetric position relative to the eyes (the head being stationary), the projection of the Helmholtz circle would fall on vertical retinal meridians in mutually asymmetric positions. Therefore, the respective visual directions would not hit corresponding retinal loci in the classical sense. Nevertheless, these loci are related to each other by simple similarity transformations (Fig. 11). In general, achieving binocular single vision of near targets off the horizontal plane of regard is more challenging since it requires precisely coordinated ocular torsions.

Appendix

For computing compounded rotations in three-dimensional Euclidean space we used the associated Clifford algebra, which is generated by three numbers, labelled $\hat{\gamma}_1$, $\hat{\gamma}_2$, $\hat{\gamma}_3$ and a unity denoted by *I*. These numbers are defined by the properties $(\hat{\gamma}_i)^2 = I$ (identity) and $\hat{\gamma}_j\hat{\gamma}_k + \hat{\gamma}_k\hat{\gamma}_j = 2\delta_{jk}I$ with $\delta_{jk} = 1$ for j =k and $\delta_{jk} = 0$ if j ≠k, whereby the indices i, j, k run from 1to 3 (Snygg 1997). Euclidian vectors are represented in this algebra by replacing the Cartesian basis vectors $\hat{e}_i$ by the Clifford numbers $\hat{\gamma}_i$ (i=1,2,3), also called the basis 1-vectors, which in turn can be conveniently represented by 4x4 Dirac matrices. The unit gaze vector $\hat{g}$, for example is represented by $\hat{g} = \sum_{i=1}^{3} g_i\hat{\gamma}_i$. The frontal, vertical and horizontal Cartesian planes, encoded by the 'plane vectors' $\hat{e}_2 \times \hat{e}_3 = \hat{e}_1, \hat{e}_3 \times \hat{e}_1 = \hat{e}_2$ and $\hat{e}_1 \times \hat{e}_2 = \hat{e}_3$ are represented by the 2-vectors $\hat{\gamma}_{23} \coloneqq \hat{\gamma}_2\hat{\gamma}_3$, $\hat{\gamma}_{31} \coloneqq \hat{\gamma}_3\hat{\gamma}_1$ and $\hat{\gamma}_{12} \coloneqq \hat{\gamma}_1\hat{\gamma}_2$, respectively. A rotation of a 1-vector x through angle χ in the plane $\hat{A} = \hat{\gamma}_{\alpha\beta}$ spanned by the 1-vectors $\hat{\gamma}_\alpha$ and $\hat{\gamma}_\beta$ with $|\hat{A}| = 1$ is obtained by the conjugation $R_A(\chi)\,xR_A^{-1}(\chi) = x'$ with the operator $R_A(\chi) = I\cos(\chi/2) - \sin(\chi/2)\hat{\gamma}_{\alpha\beta}$. The inverse of R_A is $R_A^{-1}(\chi) = R_A(-\chi)$.

Segregation of torsion from R_{exp}

Saccades from far to near space involves torsions of the eyes. This torsion interferes with the normal Donders-Listing kinematics of saccades in far viewing, resulting in a compounded rotation, which we denote R_{exp}. Denoting the Donders-Listing rotation R_{DL}, we have

$$R_{\exp} = R_F(\xi)\,R_{DL}(\rho) = \left(I\cos\xi/2 - \sin\xi/2\,\hat{\gamma}_{23}\right)\left(I\cos\rho/2 - \sin\rho/2\,\hat{\gamma}_{DL}\right) \qquad \text{(A1)}$$

Here the first expression on the right hand side is a rotation in the frontal plane, represented by the 2-vector $\hat{\gamma}_{23}$ and the second expression is a rotation in a unknown Donders-Listing plane represented by the 2-vector $\hat{\gamma}_{DL}$. To compute the torsion we evaluated the scalar products $\langle R_{\exp}, I\rangle = (R_{\exp})_0$ and $\langle R_{\exp}, \hat{\gamma}_{23}\rangle = (R_{\exp}\hat{\gamma}_{23}^{\dagger})_0$, i.e. the scalar parts of the products $R_{\exp}I = R_{\exp}$ and $R_{\exp}\hat{\gamma}_{32}$, respectively. From the two relations $u_0 = (R_{\exp})_0 = \cos\xi/2\cos\rho/2$ and $u_1 = (R_{\exp}\hat{\gamma}_{32})_0 = -\sin\xi/2\cos\rho/2$, we obtained the rotation angle ξ by eliminating the common factor $\cos\rho/2$

$\xi/2 = -\sin^{-1}\left(u_1 \Big/ \sqrt{u_0^2 + u_1^2}\right)$, with $\sqrt{u_0{}^2 + u_1{}^2} = \cos\chi/2$

The Donders-Listing rotation associated to $R_{\exp}$ then describes the torsion-free secondary or tertiary eye positions by $R_{DL}(\rho) = R_F^{-1}(\xi) R_{\exp}$.

Commutativity of Donders-Listing rotations

The orientation of the eye does not depend on the order of rotations, because Donders-Listing rotations are commutative (Fig. A1). Since these rotations are torsion-free, it suffices to compare rotations resulting from compounding a general horizontal and vertical rotation in different orders. Having done a first rotation in a horizontal, vertical or meridian direction-plane, which included the direction straight ahead, the second rotation must occur in a direction-plane perpendicular to that of the first rotation. Say, a first rotation R_H has been performed in the horizontal plane defined by the 2-vector $\hat{\gamma}_{12}$ through an angle ϑ, thence the subsequent rotation must be executed in the vertical direction-plane $\hat{\gamma}_v = R_H(\vartheta)\hat{\gamma}_{31}$. With $R_H = \left(I\cos\vartheta/2 - \sin\vartheta/2\,\hat{\gamma}_{12}\right)$ and $R_v = \left(I\cos\eta/2 - \sin\eta/2\,\hat{\gamma}_v\right)$, we obtain $R_v R_H = I\cos\chi/2 - \sin\chi/2\left\{n_2\hat{\gamma}_{31} + n_3\hat{\gamma}_{12}\right\}$, representing a rotation in the plane $\hat{\gamma}_{vH} = n_2\hat{\gamma}_{31} + n_3\hat{\gamma}_{12}$ with $n_2 = \sin\eta/2/\sin\chi/2$ and $n_3 = \cos\eta/2\sin\vartheta/2/\sin\chi/2$, through the angle $\chi = 2\tan^{-1}\left(\sqrt{1-\cos^2\eta/2\cos^2\vartheta/2}\Big/\cos\eta/2\cos\vartheta/2\right)$. Reversing the order of rotations, the first rotation is in the vertical plane defined by the 2-vector $\hat{\gamma}_{31}$ through an angle η', followed by a horizontal rotation in the direction-plane $\hat{\gamma}_h = R_V(\eta')\hat{\gamma}_{12}$. With $R_V = \left(I\cos\eta'/2 - \sin\eta'/2\,\hat{\gamma}_{31}\right)$ and $R_h = \left(I\cos\vartheta'/2 - \sin\vartheta'/2\,\hat{\gamma}_h\right)$ we obtain $R_h R_V = I\cos\chi'/2 - \sin\chi'/2\left\{m_2\hat{\gamma}_{31} + m_3\hat{\gamma}_{12}\right\}$, representing a rotation in the plane $\hat{\gamma}_{hV} = m_2\hat{\gamma}_{31} + m_3\hat{\gamma}_{12}$ with $m_2 = \cos\vartheta'/2\sin\eta'/2/\sin\chi'/2$, $m_3 = \sin\vartheta'/2/\sin\chi'/2$ through the angle $\chi' = 2\tan^{-1}\left(\sqrt{1-\cos^2\eta'/2\cos^2\vartheta'/2}\Big/\cos\eta'/2\cos\vartheta'/2\right)$. Comparing the rotation angles and plane orientations, we must have $\chi = \chi'$ and $n_i = m_i$ (i=1, 2, 3), that is $\sin\eta/2 = \cos\vartheta'/2\sin\eta'/2$ and $\cos\eta/2\sin\vartheta/2 = \sin\vartheta'/2$. We show that, under the condition of equal rotation angles $\chi = \chi'$, equal vertical components of the two differently parametrized rotation planes imply equal horizontal components and vice versa. From $\chi = \chi'$ it follows $\cos\eta/2\cos\vartheta/2 = \cos\eta'/2\cos\vartheta'/2$. Based on this identity, it follows on one hand from $n_2 = m_2$ that $\sin^2\eta/2 = \cos^2\vartheta'/2\sin^2\eta'/2 = \cos^2\vartheta'/2 - \cos^2\vartheta/2\cos^2\eta/2$, which is the same as

$\cos\eta/2\sin\vartheta/2 = \sin\vartheta'/2$, thus implying $n_3 = m_3$. On the other, it follows from $n_3 = m_3$ that $\sin^2\vartheta'/2 = \cos^2\eta/2 - \cos^2\eta'/2\cos^2\vartheta'/2$, which is the same as $\sin\eta/2 = \cos\vartheta'/2\sin\eta'/2$, thus implying $n_2 = m_2$. Conversely, it can be shown that the rotation angle of a compounded Donders-Listing rotation uniquely defines the rotation angle of the respective rotation that is obtained by reversing the order of rotation components. For this one evaluates the angles ϑ´ and η´ as a function of ϑ and η based on the relations $n_i = m_i$ (i=1, 2, 3). Taken together this shows that compounded Donders-Listing rotations represent the same torsion-free single-axis rotation irrespective of the order of the rotation components (Fig. A1).

Parameterizations of Donders-Listing rotations

One way to extract the corresponding azimuth angle from a general Donders-Listing rotation is to compare it with the following compound rotation $R_{DL} = R_v(\eta)R_H(\vartheta)$ where the first rotation, denoted R_H is a rotation in the horizontal plane of regard through an angle ϑ and the second rotation, denoted R_v is a rotation in the vertical-direction plane through an angle η. The 2-vector representing the vertical-direction plane is obtained by rotating the 2-vector representing the vertical plane through ϑ/2. With $\hat{\gamma}_v = R_H(\vartheta)\hat{\gamma}_{31}$ we obtained $\hat{\gamma}_v = -\sin\vartheta/2\,\hat{\gamma}_{23} + \cos\vartheta/2\,\hat{\gamma}_{31}$. Thus, we can write more explicitly

$$R_{DL} = R_v(\eta)R_H(\vartheta) = \left(I\cos\eta/2 - \sin\eta/2\,\hat{\gamma}_v\right)\left(I\cos\vartheta/2 - \sin\vartheta/2\,\hat{\gamma}_{12}\right). \qquad \text{(A2)}$$

To solve this equation for ϑ, we computed the scalar products $v_0 = \langle R_v R_H, I\rangle = \cos\eta/2\cos\vartheta/2$ and $v_3 = \langle R_v R_H, \hat{\gamma}_{12}\rangle = -\cos\eta/2\sin\vartheta/2$, from which we obtained $\vartheta = -2\sin^{-1}\left(v_3/\sqrt{v_0^2 + v_3^2}\right)$ and $\eta = 2\cos^{-1}\left(\sqrt{v_0^2 + v_3^2}\right)$. The angle η is the angle through which the eye would have to rotate in the vertical-direction plane to reach the experimentally determined position R_{DL}.

In an analogous way, we determined the rotation angle μ that rotates the eye in a meridian plane to the position given by the Donders-Listing rotation R_{DL} by solving the equation $R_{DL} = R_M(\mu)$ with $R_M = I\cos\mu/2 + \sin\mu/2\,\hat{\gamma}_m$. The 2-vector $\hat{\gamma}_m$ represents the meridian plane ψ =constant. It is related to the unit gaze vector by $\hat{\gamma}_m = \hat{g}\,\partial\hat{g}/\partial\varepsilon$, or explicitly $\hat{\gamma}_m = -\sin\psi\hat{\gamma}_{12} - \cos\psi\hat{\gamma}_{31}$. The rotation angle μ and the dihedral angle ψ are obtained by evaluating the respective scalar products.

Acknowledgements

We thank Carla Bettoni, Elena Buffone and Urs Scheifele for technical assistance. Hubert Misslisch works at the German Aerospace Center, Bonn, Germany. This work was supported by the Swiss National Science Foundation and the Betty and David Koetser Foundation for Brain Research.

References

Anderson-Sprecher R. Model comparison and R^2. Am Stat 48: 113-117, 1994.

Badcock DR and Schor CM. Depth-increment detection function for individual spatial channels. J Optical Soc Am [A]2: 1211-1216, 1985.

Bishop PO: Vertical disparity, egocentric distance and stereoscopic depth constancy: a new interpretation. Proc R Soc Lond B 237: 445-469, 1989.

Cumming BG. An unexpected specialization for horizontal disparity in primary visual cortex. Nature 418, 633-636, 2002.

Cumming BG, Johnston EB, Parker AJ. Vertical disparities and perception of three-dimensional shape. Nature 349: 411-413, 1991.

Dean P, Porrill J, Warren PA. Optimality of position commands to horizontal eye muscles: A test of the minimum-norm rule. J Neurophysiol 81: 735-757, 1999.

Donders FC. Beitrag zur Lehre von den Bewegungen des menschlichen Auges. Holländische Beiträge zu den anatomischen und physiologischen Wissenschaften 1: 105-145, 1848.

Fischer FP. III. Experimentelle Beiträge zum Begriff der Schichtungsgemeinschaft der Netzhäute auf Grund der binokulären Noniusmethode. In: *Fortgesetzte Studien über Binokularsehen*, edited by Tschermak A. Pflügers Archiv 204: 234-246.

Frisby JP. An old illusion and a new theory of stereoscopic perception. Nature 307: 592-593, 1984.

Haustein W. Considerations on Listing's law and the primary position by means of a matrix description of eye position control. Biol Cybern 60: 411-420, 1989.

Helmholtz H von. Handbuch der Physiologischen Optik. Hamburg: Voss, 1867.

Henriksen S, Tanabe S, Cumming B. Disparity processing in primary visual cortex. Phil Trans R Soc B 371 20150255.

Hess BJM. Dual-search coil for measuring 3-dimensional eye movements in experimental animals. Vision Res 30: 597-602, 1990.

Hess BJM, van Opstal AJ, Straumann D, Hepp K. Calibration of three-dimensional eye position using search coil signals in the rhesus monkey. Vision Res 32: 1647-1654, 1992.

Hess BJM, Misslisch H. The kinematics of far-near re-fixation saccades. J Neurophysiol 113: 3197-3208, 2015.

Hess BJM, Thomassen JS. Kinematics of visually-guided eye movements. PLoS One 9: e95234, 2014.

Hess BJM. Three-dimensional visuo-motor control of saccades. J Neurophysiol 109: 183-192, 2013.

Howard IP, Rogers BJ. Binocular vision and stereopsis. Oxford: Oxford University Press, 1995.

Jainta S, Blythe HI, Nikolova M, Jones MO, Liversedge SP. A comparative analysis of vertical and horizontal fixation disparity in sentence reading. Vision Res 110: 118-127, 2015

Mandelli M-J, Misslisch H, Hess BJM. Static and dynamic properties of vergence-induced reduction of ocular counter-roll in near vision. Europ J Neurosci 21: 549-555, 2005.

Mayhew JEW, Longuet-Higgins HC. A computational model of binocular depth perception. Nature 297: 376-378, 1982.

Minken AWH, van Gisbergen JAM. A three-dimensional analysis of vergence control at various levels of elevation. Exp Brain Res 101: 331-345, 1994.

Mok D, Ro A, Cadera W, Crawford JD, Vilis T. Rotation of Listing's plane during vergence. Vision Res 32: 2055-2064, 1992.

Nakayama K. Geometrical and physiological aspects of depth perception. In: *3-D Image Processing*, edited by Benton S, Society of Photo-Optical Instrumentation Engineers Proceedings, 20: 1-8, 1977.

King WM, Lisberger SG, Fuchs AF. Oblique saccadic eye movements of primates J Neurophysiol 56: 769-784, 1986.

Ogle KN. Researches in binocular vision. New York: Hafner Publishing Company, 1964

Panum PL. Physiologische Untersuchungen über das Sehen mit zwei Augen. Kiel: Schwerssche Buchhandlung, 1858

Prévost AP. Essai sur la théorie de la vision binoculaire. Genève: Ramboz, 1843

Read JCA, Cumming BG. Does depth perception require vertical-disparity detectors? J Vision 6: 1323-1355, 2006.

Robinson DA. A method of measuring eye movement using a scleral search coil in a magnetic field. IEEE Trans Biomed Eng 10: 137-145, 1963.

Schor C. Fixation disparity: A steady state error of disparity-induced vergence. Am J Optom and Physiol Optics 57: 618-631, 1980

Schreiber K, Crawford JD, Fetter M, Tweed D. The motor side of depth vision. Nature 410: 819-822, 2001.

Schreiber KM, Tweed DB, Schor CM. The extended horopter: Quantifying retinal correspondence across changes of 3D eye position. J Vision 6: 6, 64-74, 2006.

Schreiber KM, Hillis JM, Fillipini HR, Schor CM, Banks MS. The surface of the empirical horopter. J Vision 8: 7, 1:20, 2008.

Schumer RA and Julesz B. Binocular disparity modulation sensitivity to disparities offset of the plane of fixation. Vision Res 24: 533-542, 1984.

Siderov J, Harwerth RS, HE Bedell Stereopsis, cyclovergence and the backwards tilt of the vertical horopter. Vision Res 39: 1347-1357, 1999.

Sprague WW, Cooper EA, Tosic I, Banks MS. Stereopsis is adaptive for the natural environment. Sci Adv 1: e1400254, 2015.

Snygg J. Clifford Algebra – A Computational Tool for Physicists. New York: Oxford UP, 1997.

Stevenson SB, Schor CM. Human stereo matching is not restricted to epipolar lines. Vision Res. 37: 2717-2723, 1997.

Tweed D. Visuo-motor optimization in binocular control. Vision Res 37: 1993-1951, 1997.

Van Gisbergen JA, van Opstal AJ, Schoenmakers JJ. Experimental test of two models for the generation of oblique saccades. Exp Brain Res. 57:321-36, 1985.

Van Rijn LJ, Van den Berg AV. Binocular eye orientation during fixations: Listing's law extended to include eye vergence. Vision Res 33: 691-708, 1993.

Westheimer G. Spatial sense of the eye. Invest Ophthal and Visual 18: 893-912, 1979.

Figure Legends

Figure 1: Binocular target space. *A*: Targets lying on the intersection of two shells about the rotation-center of each eye with radius equal to the respective eye-to-target distance project onto corresponding retinal positions in the sense that they are related to each other by a similarity transformation. The locus of points in 3D fixation space defined by this intersection

is a circle, called Helmholtz circle for short. For fusion of binocular targets lying on the Helmholtz circle above or below the horizontal plane, the eyes must torque to bring the respective Donders-Listing positions (located on the white circles) into correspondence. *B*: Top view onto the intersection of the two target shells with the horizontal plane of regard. Positions along the direction-circles of the eyes (white circles in *A*, projected as lines AF_a and AF_b in *B*), which lie in the same fronto-parallel plane can meet each other by torsions of the right and left eye through appropriate angles. Abbreviations: O_a, O_b rotation centers of the right, left eye; T_a, T_b, target shells; F_a, F_b, rear fixation points; O_aO, O_bO, directions straight ahead; line AA´, Helmholtz circle projected onto the horizontal plane of regard; A, near target at the intersection of the two target shells and the horizontal plane of regard.

Figure 2: Parameterization of Donders-Listing positions by spherical polar coordinates ψ and ε. The dihedral angle ψ represents the angle subtended by the vertical plane $\hat{e}_3$ x $\hat{e}_1$ and the tilted plane $\overrightarrow{O_aN'}$ x $\hat{e}_1$. The angle ε describes the eccentricity subtended by the unit vector $\hat{g}$ and $\hat{e}_1$.

Figure 3: Binocular coordination of retinal images. *A*: The retinal images of target points in binocular fixation space, labelled H_+, A, and H_- (white dots) are projected onto the principal plane orthogonal to the horizontal plane of regard. The two target points H_+ and H_- are located at the intersections of two iso-eccentricty circles relative to straight ahead with the Helmholtz circle (h-h). *B*: Top view onto the horizontal plane of regard defined by the base line joining the rotation centers O_a and O_b and the directions straight ahead, O_aO and O_bO. The point A is at the intersection of the target shells and the horizontal plane. A_a, A_b are iso-eccentric positions in the vicinity of A. α, β, azimuth of the right, left eye. *C*: Front view onto the projected binocular targets, labelled H'_+, A´, and H'_-, in the principal plane. *D*: Side view onto the Helmholtz plane (shaded disk delineated by circle labelled C_h) with the binocular target points H_+, A and H_- and their projected images H'_+, A´ and H'_- in the principal plane (labelled p-p).

Figure 4: Relative eye-to-target distances as a function of the azimuth angles of the eyes. The triangle spanned by the eyes's rotation centers O_a, O_b, and target A with side lengths a, b, and D is similar to the shaded triangle with side lengths a´, b´and 1. Since only relative distances matter in vision, we base our analysis on the relative distances a´ and b´, which can be expressed as functions of the azimuth angles α, β and D=1.

Figure 5: Front view illustrating the trajectory of a far-to-near re-fixation saccade projected onto the principal plane. *A*. Partial view on a re-fixation saccade starting from the far fixation position of the respective eye. A_a' and A_b' represent the projected images of the far fixation positions A_a and A_b in the visual field. The two circles depict the loci of iso-eccentric positions to A_a' (black circle) and A_b' (gray circle). The intersection points define a vertical line that corresponds to the projected image of a segment of the Helmholtz circle in visual space. Note that the saccade-trajectories of the right (black curve) and left eye (gray curve) move in divergent directions from the vantage point of the fixation points in visual space. *B*. Close-up view of the initial fixation points (~50 times magnified compared to *A*). Note the vertical alignment of the fixation points. The two arcs represent the locus of iso-eccentric points relative to O'_a and O'_b; the solid vertical line represents the projected image of a segment of the Helmholtz circle. *C*. View onto the projected images of the saccade trajectories onto the principal plane from the vantage point of the near fixation points (right eye: black, left eye: gray). The saccade trajectories originate at positions close to O'_a and O'_b (see panel A) and end at disparate final positions (gray dot). The two circles represent positions iso-eccentric to the near fixation points with respect to O'_a (black circle) and O'_b (gray circle). They intersect at two points above and below the horizontal plane of regard, defining a vertical line that corresponds to the projected image of the Helmholtz circle onto the principal plane. *D*. Close-up view of the near fixation points (~46 times magnified compared to C). The saccade trajectories converge towards the intersection of the iso-eccentricity circles that appear as crossing straight lines (right eye: black, left eye: gray). Note the meandering motion of the left fixation point and its vertical alignment with the right fixation point. The solid vertical line is the projected image of an arc of the Helmholtz circle. Data from subject M1.

Figure 6: Frontal view illustrating the initial and final fixation points of far-to-near re-fixation saccades from three subjects, projected onto the principal plane. *A*. In far vision the projections of the fixation points of the right (circles, overlapped by black triangles) and left eye (black dots, overlapped by gray triangles) onto the principal plane closely overlapped. Furthermore, the Donders-Listing positions of the right (black triangles) and left eye (gray triangles) coincided with the fixation points. *B.* In near vision the Donders-Listing positions segregated from the fixation points. The dashed lines in *A* and *B* indicate the absolute horizontal and vertical positions relative to straight ahead. *C*. Same data as in B after aligning the horizontal coordinates of the fixation points. This view clearly segregated the Donders-Listing positions from the fixation points. Notice the disparate vertical positions of fixation

points. Panels in each row illustrate fixation trials from one subject collected in a single experimental session (from top to bottom M1, M2 and M3).

Figure 7: *A*. Sketch illustrating how ocular torsions achieve target fusion by rotating the dichoptic images of Donders-Listing positions towards their intersections at the Helmholtz point along iso-eccentricity circles (same nomenclature as in Figure 3A). Panels *B* to *D* illustrations of Donders-Listing and final fixation positions around the Helmholtz point (see white and gray shaded cones in *A*) at different magnifications. *B.* Frontal view onto fixation points of the right (circles, partly overlapped by black dots) and left eye (black dots) after aligning the horizontal coordinates. The circular segments labelled 'a-a' and 'b-b' depict the respective iso-eccentricity arcs drawn around the rotation centers (O'_a, open diamonds, O'_b, open squares). *C*. Close-up view (200x) of panel B illustrating the Donders-Listing positions of the right (white triangles) and left eye (gray triangles) associated to the fixation points. In this magnification, the circular segments appear as straight lines. *D*. Spread of iso-eccentricity arcs relative to the respective fixation points of the right eye (circles superimposed onto each other at coordinate origin). For comparison the relative positions of fixation points and Donders-Listing position of the left eye (black circles) are also depicted (gray triangles). *E*. Same as in *D* but for the left eye. Data from subject M1.

Figure 8: *A, B*. Vertical disparities of fixation points (right: circles, left: dots) and associated Donders-Listing positions (right: open, left: gray squares) plotted versus horizontal disparities relative to the Helmholtz point. Fixation points and Donders-Listing positions of the right eye were reflected at the vertical axis through zero to avoid overlapping (see example in first row, panel B). The straight line fits through fixation points cross each other close to the estimated Helmholtz point. Offsets of fixation points and r^2-values obtained from linear fits $f(x) = px+q$ (from top to bottom): q=-0.001° (r^2 =1.0), 0.008° (0.97), -0.00051° (0.98). Notice rotation and shifts of linear fits through Donders-Listing positions in B. *C*. Area of fusion-triangles of fixation points (circles and dots) and areas of Donders-Listing positions (white and gray squares) as a function of horizontal disparities. The fusion areas of the right eye were reflected at the vertical axis through zero. Note the parabolic increase of fusion areas as fixation-points moved away from the Helmholtz point. Parameters of parabolic fits, $f(x) = ux^2 + vx + w$ (from top to bottom): u =0.86 (r^2 =1.0), 0.72 (r^2 =0.98), 0.82 (r^2 =0.99). Note that the vertices of these parabolas were centered at zero ($|v|, |w| < 10^{-9}$). Each row illustrates fixation trials from one subject collected in a single experimental session (from top to bottom M1, M2,

and M3). The different fixation patterns were due to the different signs of signed horizontal and vertical disparities.

Figure 9: Modulation of differential half-vergence angles in comparison to ω-torsion. A to C, Examples of the average modulation (±SD) of the differential half-vergence angles of the right (δα, positive going) and the left eye (δβ, negative going). The respective average ω-torsions (±SD) are shown as gray bands. Note the variable onsets of differential half-vergence angles (black arrow heads) versus ω-torsion (gray arrowheads). The average differences in onsets for crossing the level of ±0.01° of positive/negative going traces were significant for the left eyes in A ($t = 3.2$, $p = 0.003$, $N = 25$) and B ($t = 3.8$, $p = 0.0004$, $N = 19$) and for the right eye in C ($t = 8.1$, $p < 10^{-9}$, $N = 25$). Each panel shows data from one animal in one session (from top to bottom M1, M2, and M3).

Figure 10: Top view onto the horizontal plane of regard: In the vicinity of fixated target A, the locus of positions at which the segment O_aO_b subtends a constant angle falls always between the loci of positions iso-eccentric to O_a and O_b, respectively (compare both the circular segments a-a and b-b through A, centered respectively at O_a and O_b, to the Vieth-Müller circle through A, O_a and O_b). Abbreviations: α, β, half-vergence angles; a, b, relative fixation distances; O_aO , O_bO, directions straight-ahead relative to the respective eye; p-p, principal plane viewed edge-on.

Figure 11: Front view onto the principal plane showing the projection images A, B, and C of respective fixations points on the Helmholtz circle in binocular fixation space. The image of the Helmholtz circle is a vertical line in the principal plane (gray line h-h). Note that the depicted line is much smaller than the actual diameter of the Helmholtz circle, which depends on the diameters of the target shells (not shown). For comparison a replica of the iso-eccentricity circle of target C as seen by the left eye is shown on the right side (gray circle centered at O_a). Although the vertical disparities, for example the lengths of segments $B'_aC'_a$ and $B'_bC'_b$ in the projection images of the right and left eye are different, they are similar by the intercept theorem (Thales), independent of the particular convergence state of the eyes.

Figure A1: *A*, Front view on the spherical visual field showing three different paths (in black) connecting the reference position O (in direction straight ahead) to position B, namely either directly along the meridian circle through O, B and F (=rear fixation point, not seen in front view) or indirectly via A or A´. Horizontal ellipse (in gray): upward tilted horizontal direction-circle though A´, B and F; vertical ellipse (in gray): direction-circle through A, B

and F. *B*, Top view onto the great circle through O, A and F. Straight line (in gray): projected vertical direction-circle through A, B and F; ellipse (in gray): projected horizontal direction circle through A´, B and F; $O_{a,}$ rotation center; F, rear fixation point; dashed vertical line through A: projected Helmholtz circle; ϑ: azimuth; η: elevation.

Table Legends

Table 1: Fixation positions projected onto the principal plane (mean values ±SD). The coordinate origin is the rotation center of the right eye. In sessions labelled by stars (*), only part of the fixations fulfilled the fusion criteria as indicated.

Table 2: Fixation parameters of far-to-near re-fixation saccades showing mean values ± SD The variability of the near-fixation point eccentricity was determined by computing the ratio $\rho = |R_{DL}-R_F|/R_F$ where R_{DL} and R_F were, respectively, the radii of the iso-eccentricity circles of Donders-Listing positions and fixation points. In sessions labelled by stars (*), only part of the fixations fulfilled the fusion criteria as indicated.

Table 3: Average disparities (± SD) of fixation points compared to the Donders-Listing (DL) positions. Note that vertical disparities are disparities between the positions of the right and left eye whereas horizontal disparities are disparities relative to the Helmholtz point. For comparisons absolute values are shown because signs typically changed within a session from trial to trial. In sessions labelled by stars (*), only part of the fixations fulfilled the fusion criteria as indicated.

Table 4: Areas of fusion triangles in far and near vision. The areas were obtained by Heron's formula based on the location of the fixation and Helmholtz points. Horizontal and vertical disparities relative to the Helmholtz point estimated by the offsets of linear least-squares fit of disparities in near vision. In sessions labelled by stars (*), only part of the fixations fulfilled the fusion criteria as indicated.

Footnotes

1. A 25° horizontal saccade followed by a 20° vertical saccade results in torsion of the retinal image of +4.5° compared to -4.5° if the saccade order is reversed.

2. The horizontal plane of regard is naturally defined as the plane spanned by the ocular rotation centers of the right and left eye and a fixation point at the horizon straight ahead with the head upright.

3. In geometric terms the cross product of two unit vectors, $\hat{e}_i \times \hat{e}_j$ (i ≠j) represents an oriented unit plane. Indeed the exterior product (bi-vector) $\hat{e}_{ij} = \hat{e}_i \wedge \hat{e}_j$ is related to the cross product by $\hat{e}_i \times \hat{e}_j = -(\hat{e}_i \wedge \hat{e}_j)\hat{e}_{123}$, using the 3-dimensional pseudo-scalar $\hat{e}_{123} = \hat{e}_1\hat{e}_2\hat{e}_3$.

4. Definition of the Clifford scalar product: The Clifford scalar product of x and y, denoted by $\langle x, y \rangle = \left(xy^{\dagger} \right)_0$ is the coefficient of the unity I of the Clifford product $xy^{\dagger}$ where $y^{\dagger}$ is the reverse of y (see Snygg 1997).

5. This is the sine law for a triangle with side lengths 1, a, b and angles $\alpha' = \pi/2 - \alpha$ opposite to side b and $\beta' = \pi/2 - \beta$ opposite to side a.

6. Since we considered only convergent fixations, the positions lay all in front of the subject.

7. These definitions are independent of the length of the inter-ocular distance because both a, b are distance ratios; they scale with the inter-ocular distance D.

8. The eccentricity angles ε_a and ε_b of the two points converge towards the half-vergence angles α and β for both $-\psi_a$ and ψ_b converging towards π/2.

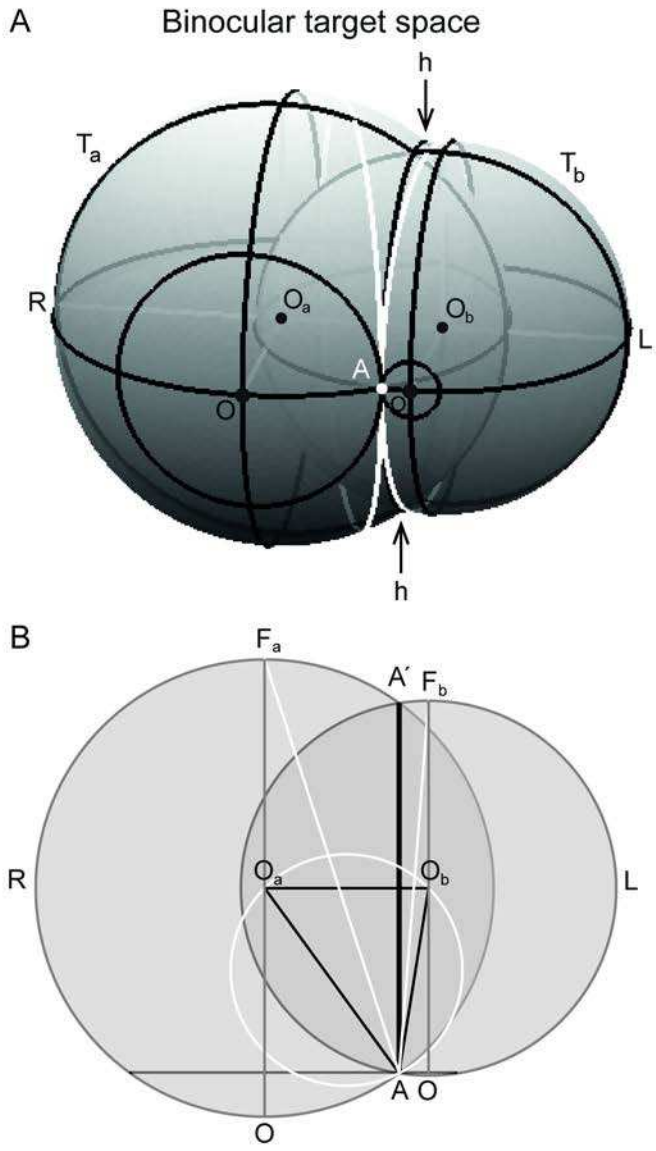
A
Binocular target space
h
T_a
T_b
R
L
O_a
O_b
A
O
h
B
F_a
A´
F_b
R
L
O_a
O_b
A O
O

Figure 1

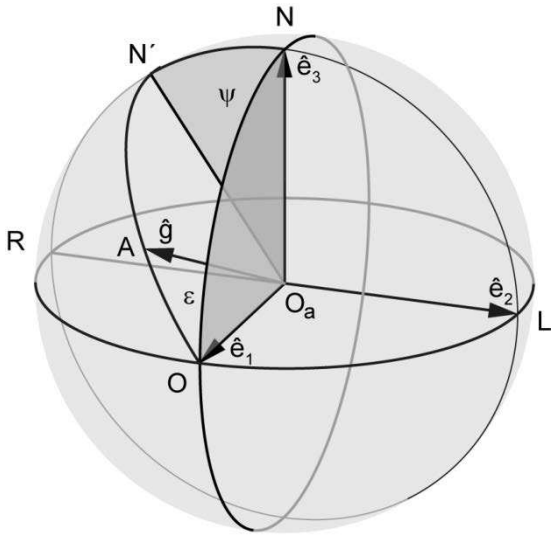

Figure 2

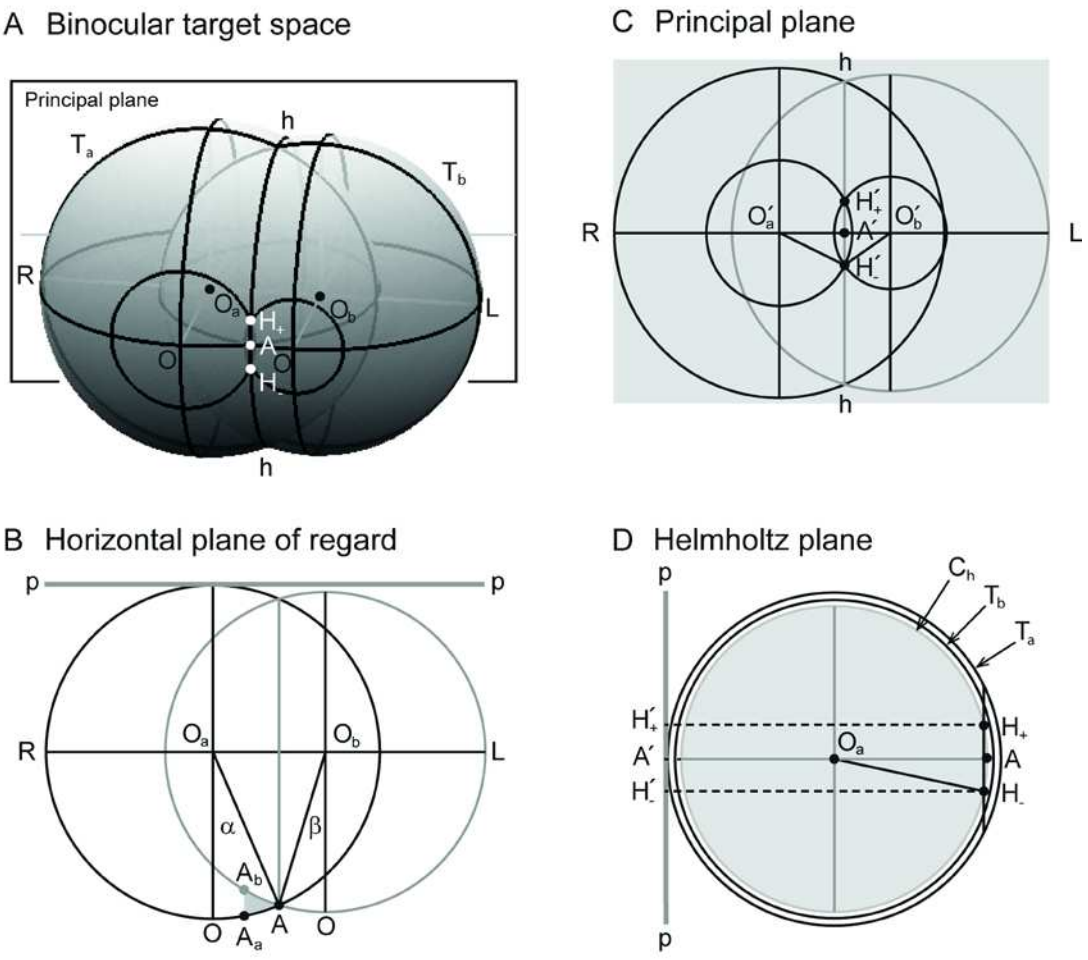
A Binocular target space
Principal plane
h
T_a
T_b
R
L
O_a
O_b
H_+
A
O
O
H_-
h
C Principal plane
h
R
L
O'_a
H'_+
A′
O'_b
H'_-
h
B Horizontal plane of regard
p
p
R
L
O_a
O_b
α
β
A_b
O
A_a
A
O
D Helmholtz plane
p
C_h
T_b
T_a
H'_+
A′
H'_-
O_a
H_+
A
H_-
p

Figure 3

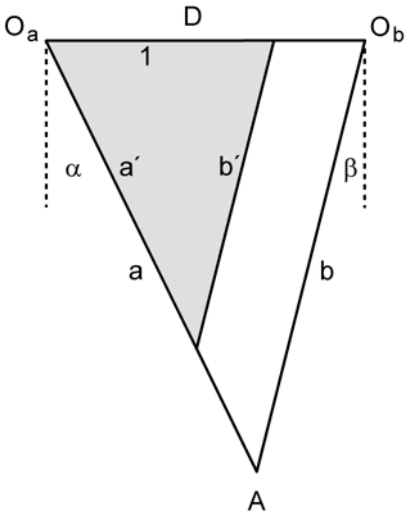

Figure 4

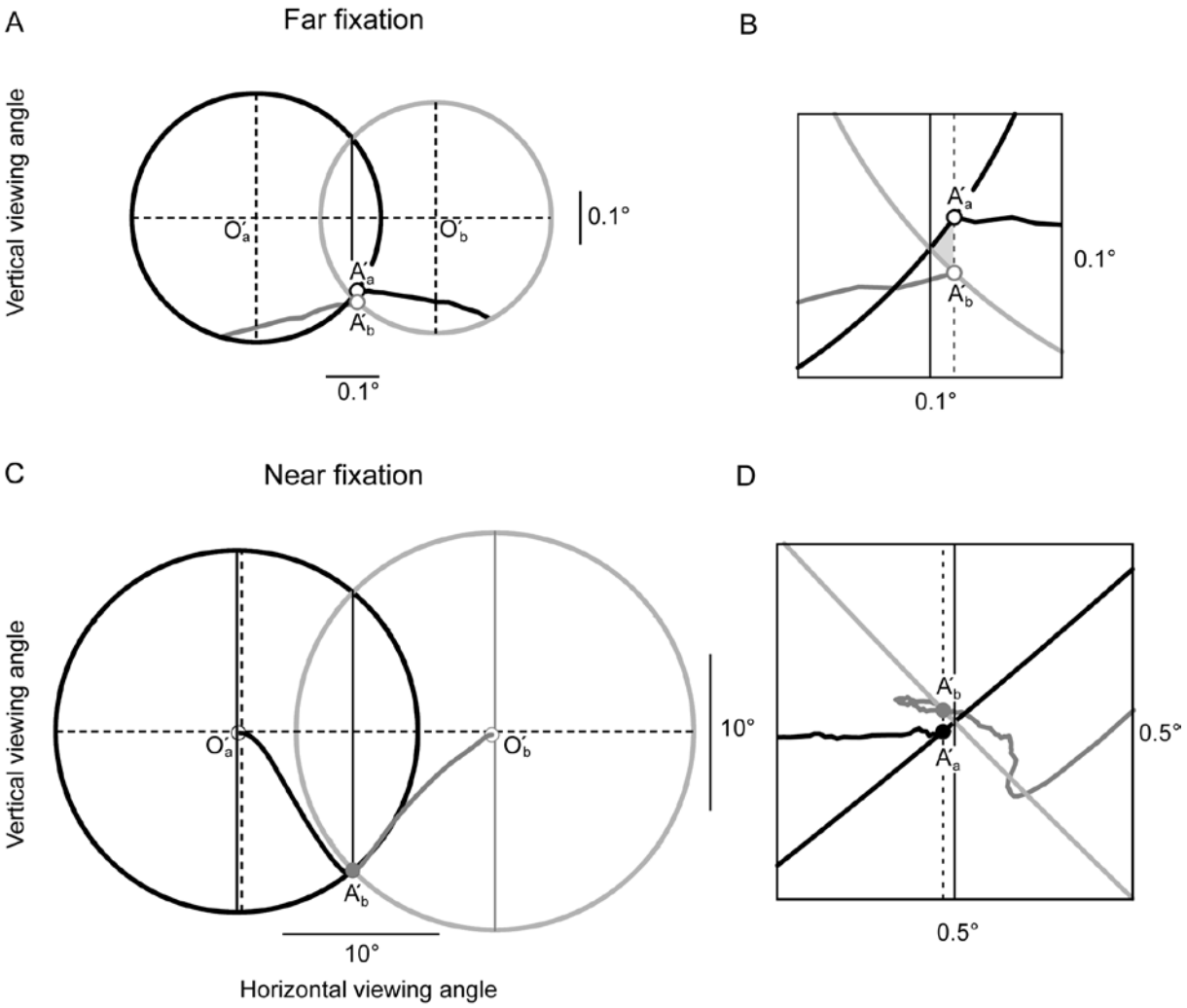
A
Far fixation
B
Vertical viewing angle
O´a
O´b
A´a
A´b
0.1°
0.1°
0.1°
0.1°
C
Near fixation
D
Vertical viewing angle
O´a
O´b
A´b
10°
10°
Horizontal viewing angle
A´b
A´a
0.5°
0.5°

Figure 5

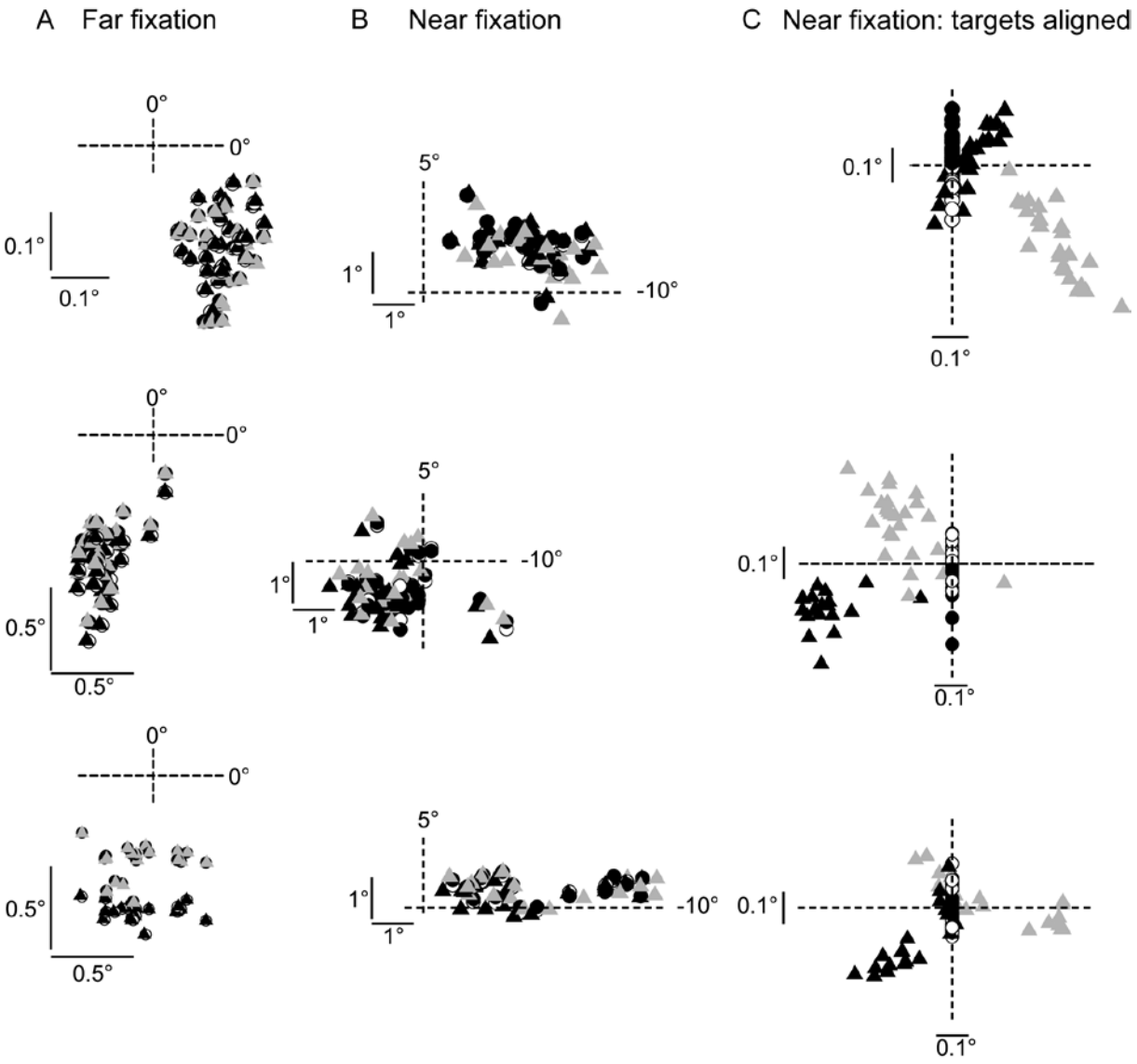
A Far fixation
B Near fixation
C Near fixation: targets aligned
0°
0°
0.1°
0.1°
5°
1°
-10°
1°
0.1°
0.1°
0°
0°
0.5°
0.5°
5°
1°
-10°
1°
0.1°
0.1°
0°
0°
0.5°
0.5°
5°
1°
-10°
1°
0.1°
0.1°

Figure 6

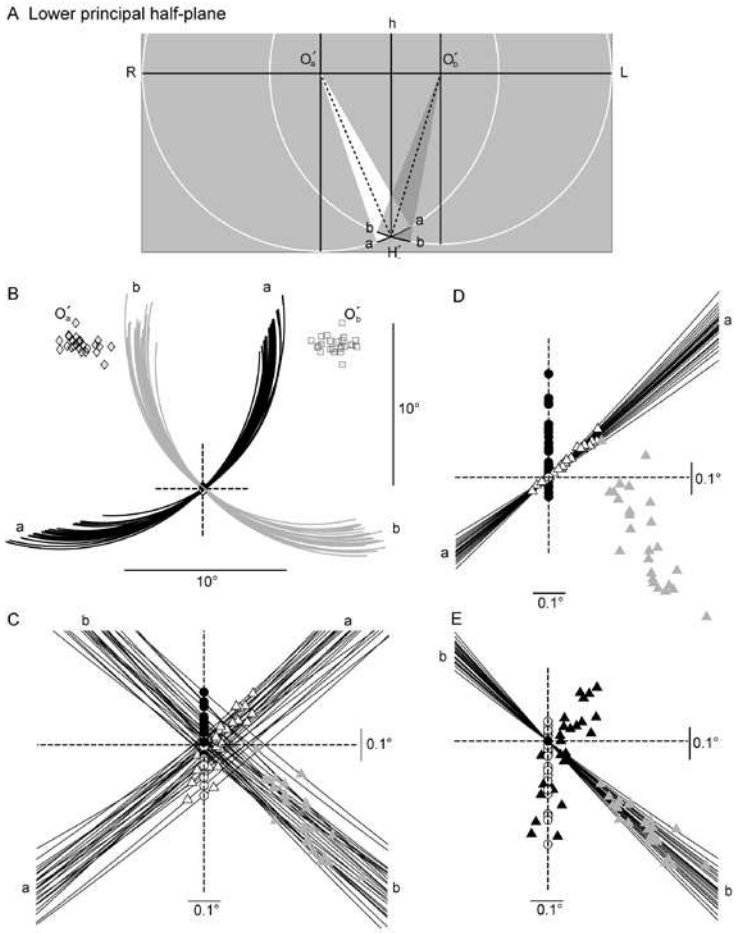

Figure 7

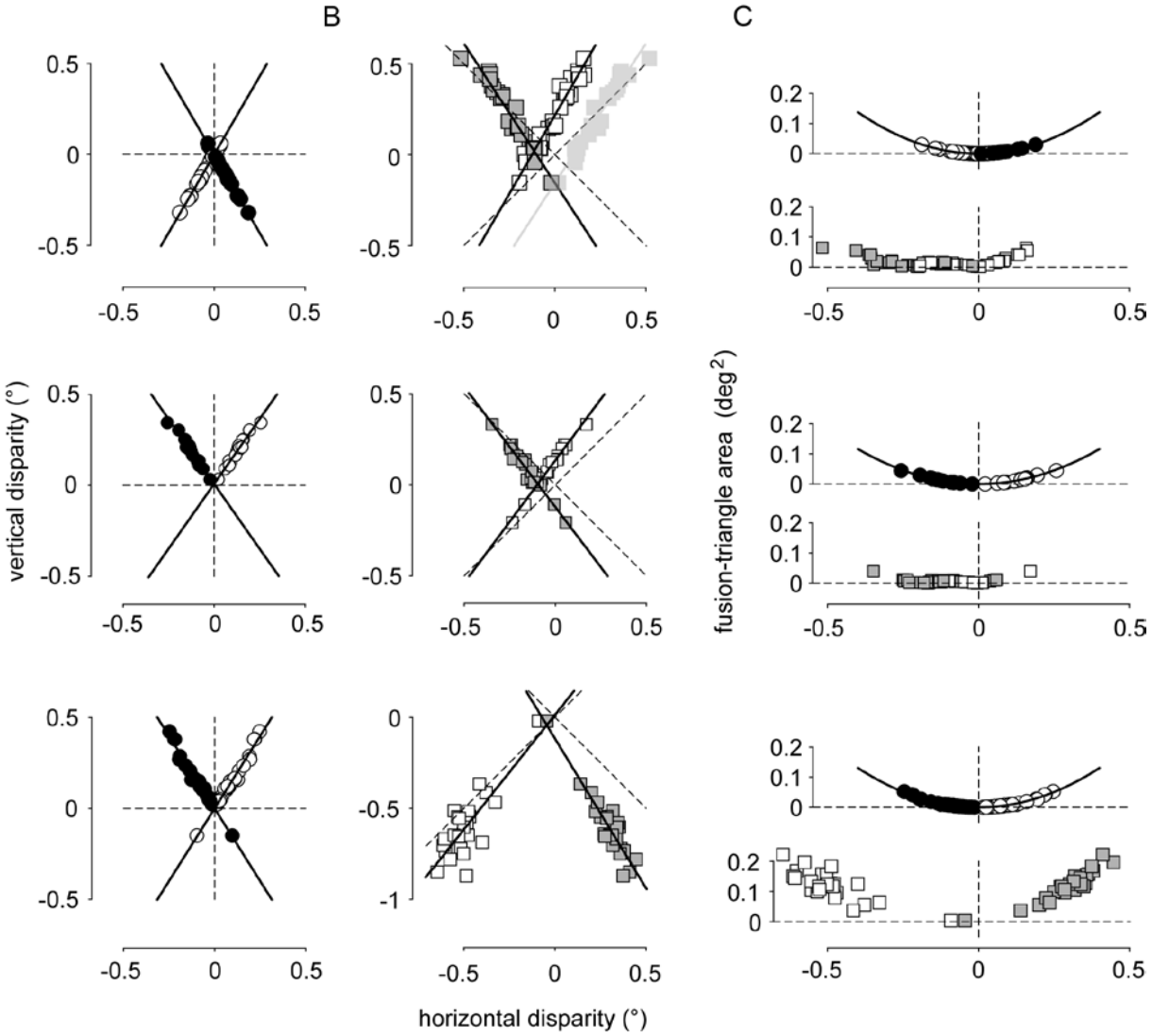
B
C
vertical disparity (°)
horizontal disparity (°)
fusion-triangle area (deg²)

Figure 8

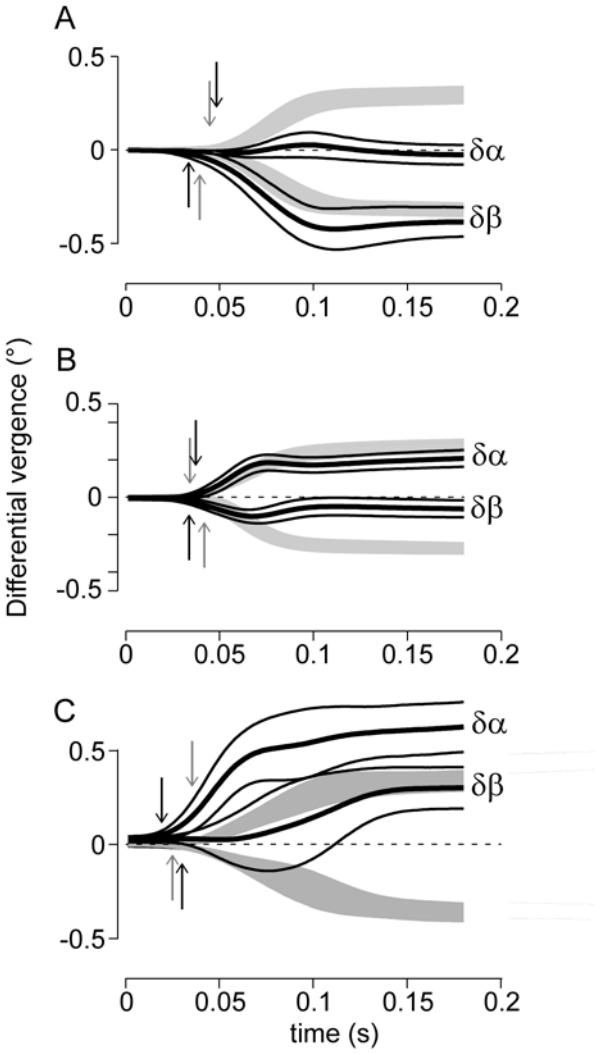

Figure 9

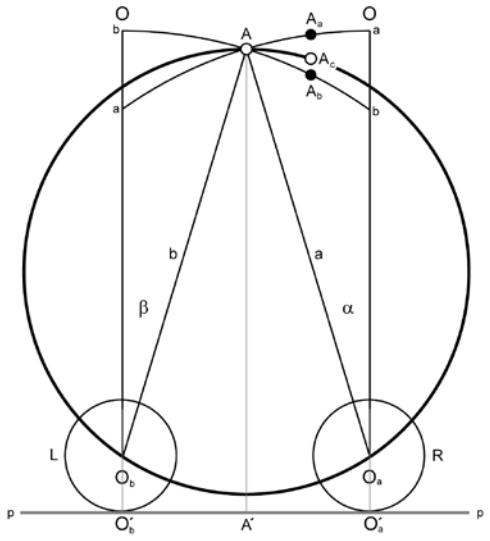

Figure 10

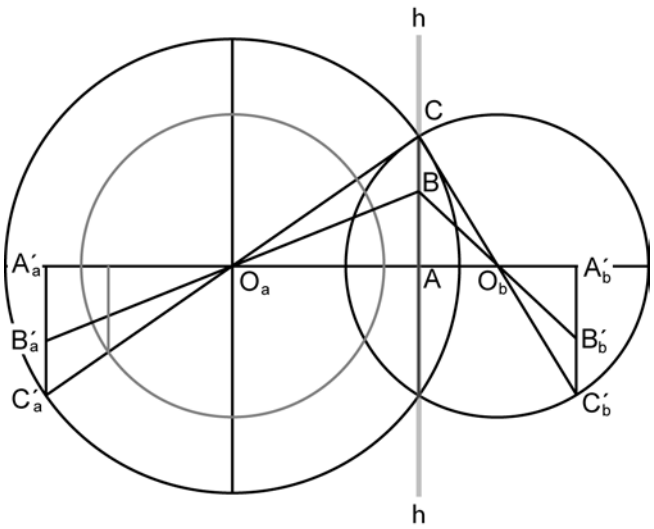

Figure 11

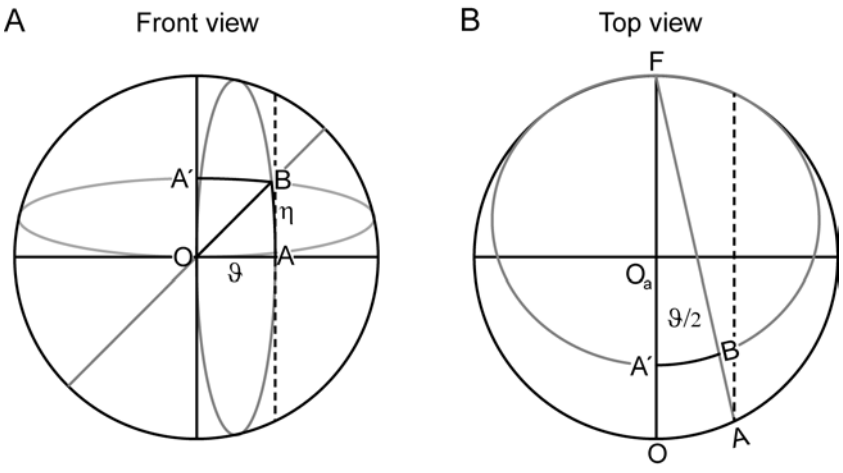

Figure A1

Table 1: Fixation positions projected onto the principal plane (mean values ±SD). The coordinate origin is the rotation center of the right eye. In sessions labelled by stars (*), only part of the fixations fulfilled the fusion criteria as indicated.

		Far fixation positions (°)			Near fixation positions (°)		
Subject	Trials	Horizontal	Vertical		Horizontal	Vertical	
Session	N	right=left	right	left	right=left	right	left
M1							
48*	5 of 11	0.2 (0.03)	-0.3 (0.03)	-0.2 (0.06)	11.6 (0.7)	- 9.4 (0.3)	- 9.3 (0.3)
49	25	0.1 (0.04)	-0.2 (0.06)	-0.2 (0.06)	7.5 (0.8)	- 8.9 (0.5)	- 8.9 (0.5)
68	07	-0.3 (0.5)	0.6 (0.2)	0.3 (0.1)	9.3 (0.6)	-10.4 (0.4)	-10.8 (0.5)
70	26	-1.8 (0.1)	0.0 (0.1)	-0.1 (0.2)	9.4 (0.8)	- 9.9 (0.7)	-10.9 (0.7)
M2							
41*	26 of 47	-0.09 (0.2)	-2.0 (0.2)	-1.8 (0.2)	10.8 (0.8)	- 9.3 (0.5)	- 9.0 (0.6)
43	27	0.0 (0.2)	-1.0 (0.2)	-0.9 (0.2)	9.1 (0.8)	- 7.4 (0.5)	- 7.0 (0.4)
44*	36 of 42	-0.15 (0.2)	-0.8 (0.2)	-0.7 (0.2)	9.5 (0.7)	-14.5 (0.6)	-13.6 (0.6)
45	25	-0.3 (0.1)	-0.8 (0.2)	-0.7 (0.2)	4.6 (0.8)	-10.7 (0.6)	-10.7 (0.6)
47	17	0.1 (0.1)	-1.7 (0.1)	-1.6 (0.1)	8.4 (0.6)	-10.5 (0.5)	-10.5 (0.5)
48	25	-0.6 (0.1)	-1.4 (0.2)	-1.5 (0.2)	8.2 (0.7)	-10.3 (0.9)	-10.4 (0.9)
52	73	-0.2 (0.1)	-1.3 (0.2)	-1.3 (0.2)	9.2 (1.0)	-12.4 (0.8)	-11.9 (0.7)
M2**							
57	14	0.1 (0.2)	-1.2 (0.2)	-1.2 (0.2)	9.2 (0.6)	10.9 (0.9)	10.9 (0.9)
59*	6 of 10	0.1 (0.1)	-1.1 (0.1)	-1.2 (0.1)	8.7 (0.8)	10.3 (0.8)	10.2 (0.7)
M3							
42	19	-0.07 (0.2)	-0.8 (0.05)	-0.5 (0.1)	7.7 (1.6)	-9.6 (0.3)	- 9.5 (0.3)

M2**: Trials with near target 10° above horizontal plane of regard.

Table 2: Fixation parameters of far- to-near re-fixation saccades showing mean values ± SD The variability of the near-fixation point eccentricity was determined by computing the ratio $\rho = |R_{DL}-R_F|/R_F$ where R_{DL} and R_F were, respectively, the radii of the iso-eccentricity circles of Donders-Listing positions and fixation points. In sessions labelled by stars (*), only part of the fixations fulfilled the fusion criteria as indicated.

		Far fixation			Near fixation				
Subjects Session	Trials N	Vergence angle (°)	Target shell R_a (°)	Target shell R_b (°)	Vergence angle (°)	Target shell R_a (°)	Target shell R_b (°)	Variability of eccentricity x10^{-4} (right)	(left)
M1									
48*	5 of 11	1.6 (0.2)	0.3 (0.03)	0.2 (0.1)	15.8 (0.4)	14.9 (0.5)	10.4 (0.5)	0.8 (0.5)	2.6 (1.0)
49	25	1.8 (0.3)	0.2 (0.04)	0.3 (0.1)	15.3 (0.9)	11.7 (0.7)	12.1 (0.6)	0.3 (0.3)	1.1 (1.1)
68	7	3.4 (2.5)	0.7 (0.3)	2.6 (2.2)	19.5 (0.1)	14.0 (0.2)	14.8 (0.7)	0.4 (0.2)	0.8 (0.6)
70	26	1.8 (0.5)	1.8 (0.1)	2.3 (0.1)	18.5 (0.4)	13.6 (0.7)	14.3 (0.9)	0.3 (0.3)	1.7 (1.0)
M2									
41*	26 of 47	2.0 (0.4)	2.0 (0.2)	1.9 (0.2)	11.2 (1.4)	14.3 (0.7)	9.2 (0.7)	0.6 (0.5)	0.5 (0.5)
43	27	1.3 (0.7)	1.0 (0.2)	1.0 (0.2)	14.8 (1.6)	11.7 (0.7)	9.3 (1.2)	1.0 (0.5)	0.5 (0.4)
44*	36 of 42	2.2 (0.6)	0.9 (0.2)	1.0 (0.2)	14.9 (1.5)	17.4 (0.6)	14.8 (1.0)	4.3 (2.5)	1.2 (0.8)
45	25	1.1 (0.4)	0.8 (0.2)	0.8 (0.2)	14.4 (0.9)	11.6 (0.7)	14.9 (0.8)	4.3 (1.4)	0.7 (0.6)
47	17	1.5 (0.4)	1.7 (0.1)	1.7 (0.1)	16.5 (0.7)	13.4 (0.3)	13.4 (0.7)	6.3 (2.7)	3.4 (1.4)
48	25	1.5 (0.5)	1.5 (0.2)	1.7 (0.2)	16.3 (0.8)	13.2 (0.8)	13.3 (0.8)	5.4 (2.4)	2.7 (1.8)
52	73	1.6 (0.3)	1.3 (0.2)	1.3 (0.2)	15.9 (0.9)	15.5 (0.9)	13.8 (0.7)	6.0 (2.4)	3.0 (1.6)
M2**									
57	14	1.4 (0.5)	1.2 (0.2)	1.2 (0.2)	16.7 (0.5)	14.3 (0.5)	13.2 (1.1)	1.0 (0.8)	3.6 (1.3)
59*	6 of10	1.5 (0.6)	1.1 (0.1)	1.2 (0.1)	15.8 (0.2)	13.5 (0.8)	12.6 (0.7)	1.4 (1.0)	4.0 (1.6)
M3									
42	19	1.5 (0.7)	0.8 (0.05)	0.8 (0.5)	12.8 (2.3)	12.4 (1.0)	11.4 (1.5)	1.2 (1.0)	0.8 (0.8)

M2**: Trials with near target 10° above horizontal plane of regard.

Table 3: Average disparities (± SD) of fixation points compared to the Donders-Listing (DL) positions. Note that vertical disparities are disparities between the positions of the right and left eye whereas horizontal disparities are disparities relative to the Helmholtz point. For comparisons absolute values are shown because signs typically changed within a session from trial to trial. In sessions labelled by stars (*), only part of the fixations fulfilled the fusion criteria as indicated.

Subject Session Nr.	Trials N	Vertical $\|\delta z\|$ (°)	Horizontal $\|\delta y\|$ (°)	DL vertical $\|\delta z\|$ (°)	DL horizontal $\|\delta y_a\|$ (°)	DL horizontal $\|\delta y_b\|$ (°)	t-test or KW
M1							
48*	5 of 11	0.05 (0.04)	0.03 (0.02)	0.3 (0.05)	0.1 (0.02)	0.3 (0.05)	$p<10^{-3}$
49	25	0.1 (0.1)	0.05 (0.05)	0.2 (0.2)	0.1 (0.05)	0.3 (0.1)	$p<10^{-3}$
68	7	0.4 (0.2)	0.2 (0.1)	0.7 (0.3)	0.3 (0.15)	0.4 (0.2)	$p<0.05$
70	26	1.0 (0.2)	0.6 (0.1)	1.3 (0.3)	0.6 (0.20)	0.8 (0.2)	$p<10^{-3}$
M2							
41*	26 of 47	0.3 (0.1)	0.2 (0.08)	0.5 (0.1)	0.4 (0.1)	0.3 (0.1)	$p<10^{-3}$
43	27	0.4 (0.2)	0.2 (0.1)	0.7 (0.2)	0.4 (0.1)	0.3 (0.1)	$p<10^{-3}$
44*	36 of 42	1.0 (0.3)	0.9 (0.3)	1.1 (0.3)	1.2 (0.3)	0.9 (0.3)	$p<0.05$
45	25	0.1 (0.08)	0.07 (0.06)	0.3 (0.1)	0.4 (0.1)	0.1 (0.07)	$p<10^{-3}$
47	17	0.08 (0.07)	0.05 (0.04)	0.9 (0.2)	0.7 (0.2)	0.5 (0.1)	$p<10^{-3}$
48	25	0.2 (0.1)	0.10 (0.07)	0.6 (0.2)	0.5 (0.1)	0.3 (0.09)	$p<10^{-3}$
52	73	0.4 (0.2)	0.3 (0.1)	0.9 (0.3)	0.9 (0.2)	0.6 (0.2)	$p<10^{-3}$
M2**							
57	14	0.1 (0.06)	0.08 (0.04)	0.25 (0.14)	0.1 (0.1)	0.3 (0.1)	$p<5\cdot10^{-3}$
59*	6 of 10	0.1 (0.08)	0.07 (0.05)	0.35 (0.13)	0.15 (0.08)	0.3 (0.1)	$p<5\cdot10^{-3}$
M3							
42	19	0.09 (0.05)	0.07 (0.04)	0.2 (0.1)	0.2 (0.1)	0.2 (0.2)	$p<0.01$

M2**: Trials with near target 10° above horizontal plane of regard. KW: Kruskal-Wallis.

In the sessions labelled by stars, only part of the fixations fulfilled the fusion criteria.

Table 4: Areas of fusion triangles in far and near vision. The areas were obtained by Heron's formula based on the location of the fixation and Helmholtz points. Horizontal and vertical disparities relative to the Helmholtz point estimated by the offsets of linear least-squares fit of disparities in near vision. In sessions labelled by stars (*), only part of the fixations fulfilled the fusion criteria as indicated.

		Average areas of fusion triangles mean (±SD)		Near fixations: least-squares linear fitting of vertical disparities as a function of horizontal disparities			
Subjects/ Session	Trials N	Far fixation (arc degree)^2	Near fixation (arc degree)^2	Horizontal offset (°)	Vertical offset (°)	slope	R^2
M1							
48*	5 of 11	0.005 (0.007)	0.001 (0.001)	0.0001	-0.0002	1.8	1.00
49	25	0.001 (0.002)	0.005 (0.007)	0.0007	-0.001	1.7	1.00
68	7	0.015 (0.03)	0.05 (0.04)	-0.0080	0.01	1.8	0.99
70	26	0.1 (0.15)	0.3 (0.1)	-0.07	0.1	1.6	0.90
M2							
41*	26 of 47	0.08 (0.07)	0.04 (0.02)	0.005	-0.006	1.3	0.90
43	27	0.01 (0.01)	0.06 (0.05)	0.04	-0.06	1.7	0.96
44*	36 of 42	0.03 (0.03)	0.5 (0.3)	0.2	-0.18	0.9	0.95
45	25	0.02 (0.02)	0.006 (0.009)	0.001	-0.001	1.4	0.99
47	17	0.01 (0.01)	0.003 (0.006)	-0.001	0.002	1.6	0.99
48	25	0.02 (0.01)	0.01 (0.01)	0.0003	-0.0005	1.6	0.98
52	73	0.01 (0.01)	0.08 (0.05)	0.03	-0.04	1.2	0.96
M2**							
57	14	0.009 (0.006)	0.006 (0.006)	0.002	0.003	-1.5	0.99
59*	6 of 10	0.01 (0.007)	0.006 (0.007)	-0.002	-0.004	-1.5	1.00
M3							
42	19	0.02 (0.01)	0.004 (0.003)	0.008	-0.01	1.3	0.98

M2**: Trials with near target 10° above horizontal plane of regard.